ACOUSTICALLY SCANNED OPTICAL IMAGING DEVICES.

Semiannual Report No. 3

1 July - 31 December 1976

Contract: N00014-76-C-0129

ARPA Order No. 2778

Program Code No. 4D10

G. L. Report No. 2675

January 1977

Gordon S. Kino
Principal Investigator
(415) 497-0205

DDC
RECEIVED
APR 12 1977
A

ACOUSTICALLY SCANNED OPTICAL IMAGING DEVICES

SUMMARY

Results obtained with the airgap convolver system are described. It is shown that the system is very suitable for use in a storage correlator; the basic problems are associated with bulk wave feedthrough and other spurious responses. Considerable progress has been made in this respect. The experimental results we have obtained, and a detailed theory of the device which we have developed, tend to indicate a possible dynamic range for the device of 60 dB , well comparable to the convolver.

The device is ideally suitable as a variable delay device, which can be externally programmed to delay signals several hundred microseconds long by times of a few microseconds. We have made preliminary demonstrations of this effect. It also is extremely useful to carry out the correlation of two signals read into it at different times, to store such signals for a fraction of a second, or, by suitable programming, to act as an inverse filter to restore distorted signals. We have, therefore, placed great emphasis on the development of this device.

An important result obtained here and in France is, of course, the very impressive optical sensitivity of the storage correlator. This is because the storage time depends radically on the leakage current caused by the light incident on the device. We have devised a new storage configuration suitable for optical imaging which is much simpler than the storage correlator configuration. We have demonstrated this new mode of operation and have shown sensitivities in the microwatt/cm^2 range.

Further development of the ZnO on Si configuration has been carried

out. P-n diode convolvers of this nature have been constructed, and development of an aluminum instead of gold technology suitable for Schottky diodes and overlay p-n diodes has been pushed forward. At the time of writing, we have succeeded in making the first ZnO on Si p-n diode storage correlator. This has storage times in the 10-20 msec range, and gives correlation between separate signals read into it within this time. Further details of these results will be given in a later report.

We have also been examining the use of gallium arsenide instead of silicon. This would give the advantage that we would not need zinc oxide in the convolver region, only on the transducers. Thus, many of the difficulties of zinc oxide would be eliminated and an extremely uniform and flexible device could be constructed. It appears that we can obtain high quality gallium arsenide from Teledyne MEC, who are extremely interested in supplying it to us for this application.

ACOUSTICALLY SCANNED OPTICAL IMAGING SYSTEM

I. INTRODUCTION

The main effort during the last six months has been devoted to the airgap convolver configuration, because (1) the airgap configuration that we described in the last report has proven to be mechanically stable and uniform, and relatively easy to assemble; (2) the use of this configuration has enabled us to experiment with a wide range of diode structures; (3) the device can be used for both storage processing and for optical imaging; (4) the initial results obtained were so encouraging that, despite the promise of the zinc oxide on silicon configuration, it seemed better to emphasize the results that could be obtained with the airgap configuration.

A main thrust of the work has involved the development of the storage correlator because of its great promise as an important signal processing device. During this period, we have demonstrated that such devices can be used as a variable delay line, and as a correlator of stored signals with signals read in at a later time.

A major step forward, during the last six months, has been the development of a complete storage correlator theory. This theory predicts the output within a few dB's and shows that the dynamic range of the device should be of the order of 60 dB, about the same as an ordinary convolver.

An important breakthrough mentioned in our previous progress reports, but developed more completely in France, has been to show that the storage correlator is inherently a device with extremely high optical sensitivity.

This is because the presence of light strongly affects the storage time of the device. We have found it possible to perform optical imaging in a simpler mode of operation than with the standard storage correlator. For this purpose, we have used the device as a standard acoustic convolver whose characteristics can be affected by a short DC pulse applied to it. By pulsing the device so as to forward bias the diodes, they become reverse biased after the end of the pulse, because of their rectification action. The reverse bias diodes are highly depleted and remain so for the storage time of the device. At the same time, the convolution output is radically decreased by 30 dB's or more during the storage time. Illumination will change the storage time and increase the convolution output. Thus, the convolver device can be used to read out an optical image in the same way as in our earlier convolver configurations, but with much better optical sensitivity. We have obtained sensitivities of the order of $1\mu w/cm^2$ with a dynamic range of 30 dB .

It will be noted that the sensitivity of this device can also be changed electronically, so that the effective dynamic range can be as much as 60 dB . This is like the use of an eye or a camera in which the pupil or lens size is changed to change the sensitivity of the device. At any one setting of the pupil, or the sensitivity control in our case, (storage time) gives an effective dynamic range of the order of 30 dB .

At the present time, the dynamic range of our storage correlator devices and those developed at Lincoln Laboratories and in France for imaging, has been limited by spurious responses. The causes of these spurious responses are due to feed-through of the readout signal directly to the output ports. These feed-through components are related to direct capacitive coupling,

- 4 -

bulk wave excitation, and direct surface wave excitation, which can excite the output transducer. Therefore, during the last few months, we have devoted considerable attention to the elimination of these feed-through problems, and have obtained extremely promising results. When we started our work, the basic feed-through levels were of the order of 25 dB below the readout signal, a level far too high to make the device a really useful signal processing device, or, for that matter, a useful optical imaging device, at least in the storage correlator mode.

The following techniques have been adopted to eliminate capacitive feed-through; (1) extremely careful attention to shielding of the device. Such measures have dropped the capacitive feed-through below the levels of the other spurious signals; (2) By using coded transducers on the $LiNbO_3$, i.e., two parallel sets of transducers which excite waves 180° out of phase on two parallel sets of diodes, we are able to eliminate most of the bulk wave feed-through; this is because bulk waves are excited in phase. This has eliminated spurious peaks in bulk wave excitation and reduced the spurious level 20 - 30 dB ; (3) By bonding the back of the $LiNbO_3$ to an epoxy backing, the spurious bulk wave level has been lowered by about the same amount. Although the results are not yet complete, the combination of the two techniques would appear to be capable of lowering the spurious levels to at least 50 dB below the main readout signal. In the end, we believe that we will be able to work with the full noise limited dynamic range of the device.

A final procedure, which was originally meant to eliminate the feed-through problem, was to place electrodes on the the top of the $LiNbO_3$, instead of on its bottom surface. These electrodes could interact directly

with the diodes. When a pulse was applied to the silicon; it was thought that they would not excite signals in the $LiNbO_3$ itself. Because of difficulties in grounding these electrodes firmly, the required reduction in feed-through was not as good as we had hoped. But this mode of operation proved two other points. First, we could lower the pulse voltages required to a few volts. Secondly, we could operate in a new convolver mode of operation and deplete the diodes to a depletion depth of 5 μm or more; this made it possible to arrive at the new optical imaging mode with which we have been experimenting recently..

We have encountered many problems with ZnO on Si configuration. One of the main ones is repeatability. This was further emphasized when a technician left Stanford and new personnel took over. Since that time, we have rebuilt the system using more science and less art. Now the results appear to be far more repeatable, with far better coupling levels than we had previously obtained. For this reason, progress has been very slow with the ZnO on Si configuration.

In addition, there has been some problem with leakage between the diodes, as has been described before, so that we have not been entirely confident on the use of p-n diodes in this configuration, although we have demonstrated in airgap convolvers that we can use p-n diodes without slots between them. Thus, we have also spent time developing Schottky diodes with aluminum gates on which ZnO can be deposited. This has required investigating the optimum temperatures for deposition of ZnO on aluminum. The results obtained have been reasonable, but not as good as we would have hoped for in this mode. We have made initial tests on new convolver configurations with our most recent development of the ZnO deposition process, and made the first demonstration of storage correlation with ZnO on Si , and storage in the p-n

diodes.

It will be seen that it is difficult to use ZnO directly on silicon in the central convolver region, although there is not too much difficulty in making transducers. We have, therefore, been investigating the use of GaAs . The advantage here is that, although ZnO is required for the transducers to obtain broad bandwidth, because GaAs is piezoelectric convolvers and storage devices can be made without the use of an additional piezoelectrical material in the central region. Such devices were demonstrated in this laboratory several years ago by Grudkowski and Quate. The problem was the lack of availability of GaAs . We have been negotiating with Teledyne MEC, who are interested in supplying us with such material, and have a first rate material facility available for this purpose. We expect, within the next few months, to demonstrate correlation devices of this kind using GaAs instead of Si , thus eliminating some of the major difficulties that we have had with the ZnO on Si configuration.

II. PRESENT STATUS

A. Storage Correlator

1. Introduction

This contract has supported work on a new airgap convolver configuration, using $4 \, \mu m$ rails of the type described in the last progress report. Because of its great importance, considerable emphasis has been placed on the application of this configuration to the storage correlator. The experimental effort has been directed at both demonstrating a practical signal processing device and using the storage process for optical imaging. Such applications require an improvement in the dynamic range through spurious signal reduction, and this has been the main thrust of our recent efforts. In addition, the theory of the device has been developed in detail, so that its operation is well understood and preformance easily calculable. The demonstration of new device applications, such as an electronically variable delay line, has been regarded as extremely important, so the results obtained so far are very encouraging.

At this time, we have not yet demonstrated a two dimensional device. This is because we regarded it as paramount to obtain a well understood device, free of spurious responses, before proceeding to work with the more complicated two dimensional devices. A two dimensional device with excessive spurious signal levels would not be capable of demonstrating a significant enough signal processing or imaging potential to warrant the development of such a device. We believe that our results are of sufficiently high quality now that we can expect to construct high performance two dimensional devices within the next six months.

- 8 -

2. Experimental work

a. Spurious signal reduction

The storage correlator readout process generates considerable spurious noise in the form of bulk waves and excited plate resonances. This reduces the usable dynamic range from a potential 50 to 60 dB to less than 25 dB.

In the present device, configuration (see Fig. 1), the major part of the readout signal potential, is developed across the $LiNbO_3$. Since the readout signals have amplitudes of several volts, considerable generation of spurious signals is to be expected. At present, four approaches to the reduction of spurious signals are being considered.

(1) Use of a cut of $LiNbO_3$ with minimum bulk wave coupling.

(2) Backing the $LiNbO_3$ with a damping material.

(3) Coding the transducers and readout signals.

(4) Placing ground strips on the upper surface of the $LiNbO_3$.

Each of these techniques is described in more detail below.

(1) Use of a cut of $LiNbO_3$ with minimum bulk wave coupling:

The $127.89°$- X propagation cut of $LiNbO_3$ has been reported to have high surface wave and low bulk wave coupling. Devices that we have fabricated on such material give slightly reduced bulk wave generation. However, this cut tends to fracture readily during processing. For these reasons, we have concluded that the benefit of using $127.89°$ $LiNbO_3$ is marginal.

(2) Backing the $LiNbO_3$ with a damping material (see Fig. 2):

As a first experiment, a 4 mil thick layer of silver epoxy was bonded to the underside of an old $LiNbO_3$ line. This resulted in significant spurious signal reduction. A working device with an epoxy backing is now

- 9 -

being fabricated.

(3) Coding the transducers and readout signals (see Fig. 3):

If half of a transducer is shifted in phase by 180° from the other half, as shown in Fig. 3, then the transducer will be insensitivite to incident straight crested plane waves; the transducer will only be sensitive to incident waves that are properly phase coded (left and right halves shifted 180° with respect to each other).

We have constructed devices with coded transducers at each end and diode arrays that are broken into two parallel halves. The 2 port loss is two dB greater than an equivalent non-coded device. The bandwidth is unchanged. Fig. 4 shows the comparative response to spurious signals. It is evident that the spurious noise is composed of plate resonances and a background. The coded fingers are not sensitive to the plate resonances. As a result, the spurious signal level in the coded device is generally lower and more constant with respect to frequency than in the device without coded transducers.

(4) Placing ground strips on the upper surface of the $LiNbO_3$ (see Fig.5);

By bringing the ground to the top of the $LiNbO_3$, the readout signal is not placed across the $LiNbO_3$. Hence, a lower amplitude is required, and the attendant spurious signal generation is reduced.

This configuration poses two problems. First, the ground strips must be firmly tied to ground, lest they radiate an rf feedthrough signal. Second, since high fields occur at the diode-ground strip interface, care must be taken to prevent breakdown.

The first problem is solved by bringing the ground strip metallization directly over the edge to the back of the line. Since the back is firmly

in contact with ground, the strips are held at ground potential along their full length.

The second problem is solved by recessing the ground strips from the $LiNbO_3$ surface and sputtering an insulating layer os SiO_2 over them.

In separate experiments, described in Sec. II, we have shown the methods discussed to be effective solutions to the problems of the top side ground strip line. However, because of the success of the alternative spurious signal reduction techniques, it has not been vital to follow up on this method. Instead, as is shown in Sec. II, we have found this approach to be an extremely useful one for optical imaging.

b. <u>New device applications</u>

We have been the only group to demonstrate the pulse mode of operation with a p-n junction storage correlator. This mode allows the demonstration of some interesting device applications, specifically as an electronically variable delay line for analog signals of arbitrary length.

The pulse mode of operation is shown in Fig. 6. Here an acoustic signal's phase and amplitude information is stored in the diode array when the diodes are forward biased by a pulse applied to the silicon. The pulse must be $\gtrsim 50$ volts and < 10 nsec . We have found avalanche transistor circuits to be a very cheap and convenient way of generating such pulses.

There had been some question as to whether p-n junctions can respond to such short pulses. With a storage correlator, the diode current must rise in response to a sharp voltage rise. The p-n junction forward bias transient current has a $t^{-\frac{1}{2}}$ characteristics, so that, for t small, the current, indeed, rises rapidly with time. (It is the voltage which changes slowly with time, because minority carriers are available and free to drift

- 11 -

across the depletion layer. This leads to the common assumption that p-n junction diodes are "slow".)

Correlation of Barker Codes   Fig. 7 shows the results of an experiment in which biphase Barker codes have been stored with the pulse mode and read out after a storage interval. The sidelobes are within $\pm$ 2 dB of theoretical values. This is ample evidence that the diodes are responding to 100 MHz signals.

Variable delay line   One novel application for the storage correlator is as an electronically variable delay line for analog signals of arbitrary length, as shown in Fig. 8. Here, the pulse mode is used to store a short acoustic pulse at the position Z_0 . This is equivalent to storing $\delta(Z-Z_0)$. If the readout signal is $G(t)$, then the output at the transducer will be $G(t) * \delta(Z-Z_0)$. Hence, delays of 0 to L/v , where L is the diode array length, may be obtained. The length of $G(t)$ is limited only by the diode storage time, which is typically several milliseconds.

We see considerable potential for a delay device of this sort. In ECM , this might serve as a delay for repeat jammers. In multielement electronically focused imaging arrays for use in nondestructive testing, programmed delays could be provided to individual elements with a minimum of timing circuitry.

3. Theoretical Work

   a. Introduction

During the last six months we have developed a theory to describe the pulse mode of operation. The following section gives a comprehensive description of the theory.

The basic model which has been adopted for the storage correlator uses the circuit shown in Fig. 9(a). V_p is the voltage applied to the central electrode, and C_p the capacity between that electrode and the diode, respectively. V_a, C_a are the corresponding quantities applied to the diode from the acoustic ports.

If we suppose that a short pulse V_p is applied at the electrode, the diode is turned on and the capacity charges up to an approximate charge $Q_p = V_p C_p$. When the pulse is turned off, the diode is turned off and can only lose charge by leakage current, so the charge is stored in the capacitor. In general, if voltages are applied to both the acoustic port and the electrode, one obtains a stored charge which depends on the weighted sum of the two applied voltages. When the diode is turned off after the short applied pulse is removed, this charge is distributed among the plate capacitor and the reverse bias capacity of the diode, which is now reverse biased. This reverse biased capacity varies with the amount of charge, for the diode behaves as a varactor. So the diode capacity depends on the original applied voltages. This is how the information is stored in the diodes.

If now, on readout, a pulse is applied at the plate, it will produce a voltage across the diode capacitor, which in turn excites an acoustic signal on the delay line through the capacitor C_a. The signal excited on the acoustic delay line will itself depend on the capacitance of the diode, and, hence, on the charge stored in the diode. By going through a procedure to determine the actual voltages involved and the power excited in the acoustic wave, one can complete the analysis and determine the actual levels which occur in the system.

- 13 -

b. Storage Correlation Theory

Charging

We begin by adopting a suitable circuit model with reasonable simplification. This model may be analyzed.

(i) Circuit Model

The complete model is shown in Fig. 9(a).

The acoustic and plate circuits are coupled only to the extent that the diode current is the sum of the currents flowing through C_a and C_p. Hence, ignoring R_p and R_a as small,

$$C_p \frac{d}{dt} (V_p - V_D) + C_a \frac{d}{dt} (V_a - V_D) = I_D .$$

This is rewritten as:

$$C \frac{d}{dt} (V_s - V_D) = I_D \qquad\qquad (1\text{-}1)$$

where

$$C = C_a + C_p$$

$$V_s = C_a/C \cdot V_a + \frac{C_p}{C} V_p .$$

Equation (1) describes the simplified equivalent circuit of Fig. 9b. Here,

$$C_D = \sqrt{\frac{2qN_D\epsilon_s}{(V_B - V_D)}} \;,\; \text{where} \; Q_D = C_D(V_D - V_B) \; \text{and} \; I_{DO} \simeq I_s e^{\beta V_D} .$$ This model holds Schottky diodes and p-n junctions operated in the memory correlator mode, that is, as fast <u>charging</u> devices.

- 14 -

(ii) Circuit Characteristics

Figure 9b yields the explicit form of Eq. (1):

$$C \frac{d}{dt} (V_s - V_D) = \frac{dQ_D}{dt} + I_s e^{\beta V_D} \quad .$$ (1-2)

If we say $Q_D = C_D(V_D - V_B)$, then Eq. (2) may be written as:

$$e^{-\beta V_B} \frac{d}{dt} \left[C(V_S - V_B) - (C_D + C)(V_D - V_B) \right] = I_s e^{\beta(V_D - V_s)} .$$ (1-3)

By defining charges:

$$\left. \begin{array}{l} Q_1 = (C_D + C)(V_D - V_B) \\ \\ Q_s = C(V_s - V_B) \end{array} \right\}$$ (1-4)

$$e^{-\beta V_B} \frac{d}{dt} \left[Q_s - Q_1 \right] = I_s e^{\beta \frac{Q_1}{C_D + C}}$$

setting $Q = Q_s - Q_1$, we have:

$$\frac{d}{dt} [Q] = I_s e^{\beta \left[\frac{-Q}{C_D + C} + \frac{Q_s}{C_D + C} + V_B \right]}$$ (1-5)

Note that, when $V_s = 0$, Q is the charge in the parallel combination of C and C_D. Integrating, we find:

$$Q = \frac{C_D + C}{\beta} \ln \left\{ \frac{\beta I_s e^{+\beta V_B}}{C_D + C} \int e^{\beta \frac{Q_s}{C_D + C}} \, dt + 1 \right\}$$ (1-6a)

Equation (1-6) is the charge equation of the device. After V_a and V_p are off, most of the stored charge resides in the diode, since $C_D \gg C_p$.

- 15 -

Hence Q gives the stored charge in terms of the source term, Q_s .

Eq.(1-6a) can also be stated in terms of voltage

$$V_D = \frac{C}{C + C_D} V_s - \frac{1}{\beta} \ln\left[\frac{\beta I_s}{C_D + C} \int e^{\beta \frac{CV_s}{C_D + C}} dt + e^{-\beta \frac{C}{C_D + C} V_B}\right] \qquad (1\text{-}6b)$$

In most cases, the second term in the $\ln$ is vanishingly small, so for the practical range of operation, the diode voltage is given by:

$$V_D(t) = \frac{C}{C + C_D} V_s(t) - \ln\left[\frac{\beta I_s}{C_D + C} \int e^{\beta \frac{CV_s}{C_D + C}} dt\right] \qquad (1\text{-}7)$$

The kernel of the integral has a sharp peak at the maximum of V_s . Writing

$$\frac{\beta C}{C + C_D} V_s(t) = \frac{\beta C}{C + C_D} \left[\frac{C_a V_a}{C_a + C_p} + \frac{C_p V_p}{C_a + C_p}\right]$$

and assuming

$$V_a = V_{ao} \sin(\omega_a t + k_a z)$$

$$V_p = V_{po} \sin(\omega_p t)$$

(with $\dfrac{C_p V_{po}}{C_a + C_p} > \dfrac{C_a V_{ao}}{C_a + C_p}$ to give well defined peak) and writing $t = t_p + \Delta$

(expanding about the peak)

$$V_s(t) = V_s(t_p) - \frac{\Delta^2}{2} f(t_p)$$

- 16 -

where

$$f(t_p) = \frac{C_a \omega_a^2}{C_a + C_p} V_{ao} \sin(\omega_a t_p + k_a z) + \frac{C_p \omega_p^2}{C_a + C_p} V_{po} \sin \omega_p t_p \quad .$$

Hence,

$$\int e^{\beta \frac{C V_s}{C_D + C} dt} \, dt = e^{\beta \frac{V_s(t_p)}{C + C_D}} \int_{-\infty}^{\infty} e^{-\alpha^2 \Delta^2} d\Delta \quad ; \quad \alpha = \sqrt{\frac{\beta C_a f(t_p)}{2(C + C_{Dp})}}$$

$$= \sqrt{\frac{2\pi(C + C_{Dp})}{3 \, C \, f(t_p)}} \, e^{\beta \frac{C V_a(t_p)}{C + C_D}}$$

(1-8)

where C_{Dp} is $C_D \big|_{t = t_p}$.

Combining (7) and (8), we get the diode voltage as a function of time.

$$V_D(t) = \frac{C}{C + C_D} \left[V_s(t) - \frac{C + C_D}{C + C_{Dp}} V_s(t_p) \right] - \frac{1}{\beta} \ln \left[\sqrt{\frac{2\pi\beta(C + C_{Dp})}{C \, f(t_p)}} \cdot \frac{I_s}{C_D + C} \right] \cdot \quad (1-9)$$

After $V_s = 0$, the diode voltage has a positive constant term (represented by the $\ln$) and a negative term (represented by $- \frac{C}{C + C_{Dp}} \cdot V_s(t_p)$. If V_D (t such that $V_s = 0$) < 0, the diode will store charge. We assume that the equivalent circuit model, when the sources turn off, is represented by Fig. 9c . Assuming $C_D \gg C_p$, we may assume most of the original stored charge resides in the diode. The stored charge is

- 17 -

$$Q = Q_D + Q_C = \left[C_D(V_D - V_B) + C_{DO}V_B\right] + C(V_s - V_D)$$

when $V_s = 0$, $Q = (C_D - C)V_D + (C_{DO} - C_D)V_B =$

$$C\frac{(C_D - C)}{(C_{Dp} + C)} V_s(t_p) + V_B(C_{DO} - C_D) + \frac{C_D - C}{\beta} \ln\left[\frac{I_s}{C_D + C}\sqrt{\frac{2\pi\beta(C + C_{Dp})}{C\,f(t_p)}}\right]$$

$$(1\text{-}10)$$

From (1), we see that the term giving the acoustic charge stored, that is, the stored information is

$$Q_a = C_a\left(\frac{C_D - C}{C_{Dp} + C}\right)V_a \qquad . \tag{1-11}$$

Readout

(i) Diode voltage due to readout signal. Fig. 9d shows the equivalent circuit; equation (1-11) gives the charge stored in C_D due to readin. ϕ_{pr} is placed across the diode through C_p . The voltage appearing across C_D transduces a surface wave. We assume $V_D < 0$, so the diode remains reverse biased. With this model, the readout will be nondestructive, since no conduction current can flow.

The net diode charge is

$$Q_D = -C_D(V_B - V_D) + C_{DO}V_B = -C_{DO}V_B\left(\frac{C_{DO}}{C_D} - 1\right) \tag{1-12}$$

- 18 -

(with $\quad C_D = \sqrt{\dfrac{2qN_D \epsilon_s}{(V_B - V_D)}} \quad ; \quad C_{DO} = C_D \big|_{V_D = 0} \quad)$.

From (10), (11) and (12), we find

$$\frac{1}{C_D} = \frac{Q_a + Q_O}{C_{DO}^2 V_B}$$

where Q_a is given by (1-11) and Q_O contains all charge terms independent of V_a .

Since

$$V_D = \frac{C_p}{C_p + C_D} \phi_p \approx \frac{C_p \phi_p}{C_D} \approx \frac{C_p \phi_p (Q_a + Q_O)}{C_{DO}^2 V_B}$$

with $\phi_p = \phi_{pO} \sin \omega_p t$, Q_a as given in (1-11), and $V_a = V_{aO} \sin(\omega_a t_p - k_a z) \times$ $\mathrm{sinc}\, \dfrac{k_a \delta}{2}$, where the $\mathrm{sinc}\, \dfrac{k_a \delta}{2}$ is due to the finite diode width, we the diode voltage is

$$V_D = \frac{C_a C_p}{2C_{DO}^2} \left(\frac{V_{aO} \phi_p}{V_B} \right) \left(\frac{C_D - C}{C_{Dp} + C} \right) \mathrm{sinc} \frac{k_a \delta}{2} \left\{ \cos[\omega_r t - (\omega_a t_p - k_a z)] - \cos[\omega_r t + (\omega_a t_p - k_a z)] \right\}$$
$$+ V_{\text{non-acoustic}}.$$

The relevant components - those representing forward and backward traveling waves are:

$$V_{Da}^{\pm} = \left(\frac{V_{aO} \phi_p}{V_B} \right) \left(\frac{C_a C_p}{2C_{DO}^2} \cdot \frac{(C_D - C)}{C_{Dp} - C)} \right) \mathrm{sinc} \frac{k_a \delta}{2} \cos \left[\omega_r t \mp (\omega_a t_p - k_a z) \right] \quad (1-13)$$

- 19 -

(ii) Coupling of array to surface wave:

We begin with Kino-Auld Eq. (31):

$$\frac{\partial a}{\partial z} + j\beta a = \frac{j\omega\rho_s \phi_1^* w}{4P_1} \quad .$$

Multiplying by ϕ_1 , with $\phi_a = a\phi_1$; $\phi_1^* \phi_1 = 2P_1 Z_o$, where

$$Z_o = 2\left|\frac{\Delta v}{v_a}\right| e^{-2\beta h}/\omega w(\epsilon_o + \epsilon_p) \quad ,$$

$$\frac{\partial \phi_a}{\partial z} + j\beta \phi_a = \frac{j\omega Z_o w \rho_s}{2}$$

we write $\rho_s = C_a \phi_s = C_a(\phi - \phi_a)$, where $C_a = \dfrac{\epsilon_o \beta}{M(\beta h)}$. With this, and writing $\gamma = \omega w C_a Z_o/2$,

$$\frac{\partial \phi_a}{\partial z} + j(\beta + \gamma)\phi_a = j\gamma\phi \tag{1-14}$$

Assuming $\phi_a = f(z)e^{-j(\beta+\gamma)z}$, and noting that $\gamma \sim C_a(\omega)$, so γ is nearly constant in ω (see Fig. 10), we find after substitution and integration:

$$\phi_a(z,\omega) = j\gamma \int \phi \, e^{j(\beta+\gamma)(z'-z)} dz' \quad .$$

*B. A. Auld and G. S. Kino, IEEE Trans. on Electron Devices, ED-18, 898-908, Oct. 1971.

The Fourier transform to the time domain is (with $\beta = \omega/v_a$):

$$\phi_a(z,t) = j \frac{\gamma e^{-j\gamma z}}{\sqrt{2\pi}} \int \left\{ \int \psi(\omega, z') e^{j\omega\left(t - \frac{z - z'}{v_a}\right)} d\omega \right\} e^{j\gamma z'} dz'$$

Hence:

$$\phi_a(z,t) = j \gamma e^{-j\gamma z} \int \phi\left(z', t - \frac{z - z'}{v_a}\right) e^{j\gamma z'} dz' \qquad (1\text{-}15)$$

Equation (1-13) gives the diode potential as of a function of z. A Fourier expansion of (1-13) gives the continuous β component that may be applied in (15).

We write:

$$V_{Da}^{\pm}(z) = e^{-j\beta z} V_p(z)$$

where $V_p(z)$ is periodic with the diode array periodicity, and $V_p(z) = V_o$, $0 \leq z \leq \delta$; $V_p = 0$ otherwise, where δ is the diode width. Then, writing:

$$V_p(z) = \sum_{n=-\infty}^{\infty} a_n e^{-j \frac{2\pi m z}{L}}$$

with

$$a_n = \frac{1}{L} \int_0^L V_p(z) e^{j \frac{2\pi m z}{L}} \quad,$$

we find:

- 21 -

$$V_p(z) = \frac{\delta V_{po}}{L} \sum_{n=-\infty}^{\infty} \text{sinc}\left(\frac{\pi m \delta}{L}\right) e^{j\frac{2\pi m}{L}\left(z + \frac{\delta}{2}\right)} \quad .$$

Retaining the $n = 0$ term, and with $\delta/L = 1/2$,

$$V_{Da}^{\pm}(z) = e^{-j\beta z} V_{po}/2 \quad .$$

Combined with (1-13),

$$V_{Da}^{\pm}(z) = \left\{ \frac{C_a C_p}{4 C_{DO}^2} \frac{C_D - C}{C_{D_p} + C} \frac{V_{ao} \phi_{pr}}{V_B} \text{sinc} \frac{k\delta}{2} \right\} \text{Re} \left\{ e^{-j(\beta z \mp \omega_r t - \omega_a t_p)} \right\}$$

$$(1\text{-}16)$$

$$= V_o \text{Re} \left\{ e^{-j(\beta z \mp \omega_r t - \omega_a t_p)} \right\}$$

If we assume that the writing wave had also been perturbed, so that its wavenumber was also $\beta + \gamma$, we find upon substituting (1-16) into (1-15),

$$\phi_a = j \gamma e^{-j\gamma z} \int V_o e^{j(\omega t - \beta z)} dz'$$

$$= \left(j \gamma V_o e^{-j\gamma z} e^{j(\omega t - \beta z)} \right) \cdot z \quad .$$

The output power is $P_{ao} = \phi_a^* \phi_a / 2 Z_o$. Hence,

$$P_{ao} = \frac{(\gamma V_o z)^2}{2Z_o} \quad .$$

Since the original acoustic input power was $P_a = \dfrac{V_{ao}^2}{2Z_o}$,

$$P_{ao} = \left\{ \frac{C_a C_p}{8qN_D \epsilon_s} \left(\frac{C_D - C}{C_{D_p} + C} \right) \gamma \phi_{pr} z \, \mathrm{sinc} \, \frac{k\delta}{2} \right\}^2 P_a \qquad (1\text{-}17)$$

where we set $C_{Do}^2 = 2qN_D \epsilon_s / V_B$. The terminal output, in dBm , is:

$$P_{ao}(dBm) = 20 \log \left\{ \frac{\phi_{pr} z \gamma}{8qN_D \epsilon_s} \left(\frac{C_D - C}{C_{Dp} + C} \right) C_a C_p \, \mathrm{sinc} \, \frac{k\delta}{2} \right\} + 10 \log P_a(mW) - I.L. \quad .$$

$$(1\text{-}18)$$

(iii) Numerical Estimates of performance.

Here, all the quantities required to evaluate (1-18) are found. The numbers are typical for our device.

$$\underline{C_a} = \epsilon_o \beta \, \frac{1 + \epsilon_p / \epsilon_o}{1 + \dfrac{e_p}{\epsilon_o} \beta h}$$

Here, we take $h = 1500 \, \overset{o}{A}$, $\nu = 100$ MHz , $C_a = 3.47 \cdot 10^{-9} \dfrac{F}{cm^2}$,

$\underline{C_p} = \epsilon_p / d$. $d = 18$ mils $= 0.045$ cm ; $\epsilon_p = 70 \, \epsilon_o$, $C_p = 1.38 \cdot 10^{-10} F/cm^2$,

$$\underline{qN_D\epsilon_s} = (1.602\cdot10^{-19} \text{ coul})(5\cdot10^{14} \text{ 1 cm}^2)(1.02\cdot10^{-12} \text{ F/cm}) =$$

$$= 8.17\cdot10^{-17} \text{ coul}^2/\text{cm}^4\text{V} \quad.$$

$$\underline{C} = C_a + C_p = 3.61\cdot10^{-9} \text{ F/cm}^2 \quad,$$

$$\underline{V}_B = \frac{kT}{q} \ln\left(\frac{N_a N_D}{n_i^2}\right) = 0.0259 \ln\left(\frac{10^{20}\cdot5.10^{14}}{(1.6\cdot10^{10})^2}\right) = 0.85 \text{ volts}$$

$\underline{I}_s$:   assume a value $\sim 5\cdot10^{-10}a/\text{cm}^2$,

$\underline{\omega}$: $2\pi\cdot10^8 \text{ Hz} = 6.28\cdot10^8 \text{ rad/sec}$,

$\underline{\beta}$: $\dfrac{\omega}{v_a} = \dfrac{6.28\cdot10^8}{3.48\cdot10^5} = 1.81\cdot10^3 \text{ cm}^{-1}$,

$\underline{\delta} = 4\mu m$

$$\text{sinc } \frac{k\delta}{2} = \text{sinc } \frac{(1.81\cdot10^3)(4.10^{-4})}{2} = 0.98$$

$$\underline{Z}_o = \frac{2\left|\dfrac{\Delta v}{v_a}\right|e^{-2\beta h}}{\omega w(\epsilon_o + \epsilon_p)} = \frac{1.60\cdot10^{10}}{v} \quad; \quad \left|\left(\frac{\Delta v}{v}\right)\right| = 0.024; \quad h = 1500 \text{ \AA} \quad,$$

$$\omega = 0.1 \text{ cm}$$

For $v = 10^8 \text{ Hz}$, $Z_o = 160 \ \Omega$.

$$\underline{\gamma} = \frac{\omega w C_a Z_o}{2} \qquad \text{for} \quad \omega = 2\pi \cdot 10^8 \text{ rad/sec} ,$$

$$w = 0.1 \text{ cm}$$

$$C_a = 3.47 \cdot 10 - 9F/cm^2$$

$$Z_o = 160 \, \Omega ,$$

$$\gamma = 17.4 \text{ cm}^{-1} .$$

A graph of (1-18) using these numbers is shown in Fig. 10. In the plotting program, P_{ao} is assumed, as is V_p . Using $(P_{ao} - I.L./2)$, $(P_{ao}$ minus the first transducer loss) and the Eq. below (1-7) , $V (t_p)$ is found. With $\omega_a = \omega_p$, this gives $f(t_p)$ and the $\ln$ term in (9), as well as C_{Dp} . Setting $V_s(t) = 0$ in (9) gives V_D and, hence, C_D . With C_D , C_{Dp} and P_a , (1-18), the output power, is found.

For $P_{ao} = 22$ dBm , $z = 2$ cm $\phi_{pr} = 2v$ $V_p = 250$ volts, IL = 20 dB (volts) = 10 dB (power), $P_{ao}(dBm) = -27.9$ dBm .
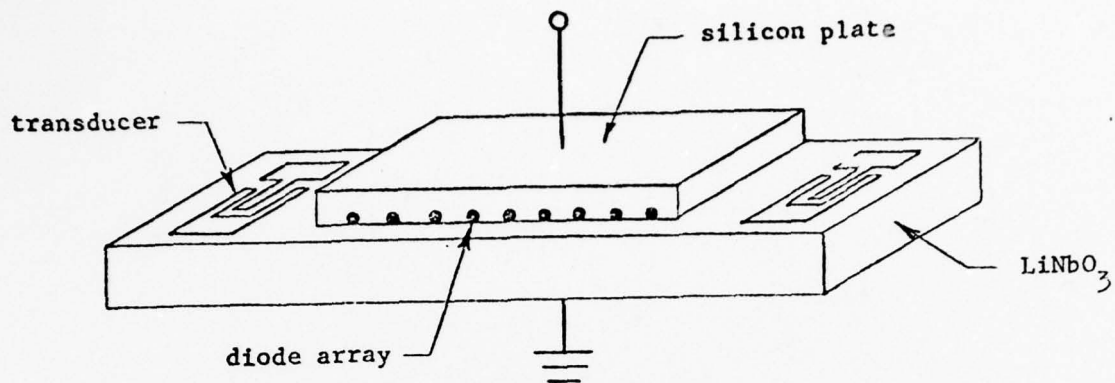
Fig. 1.   The Memory Correlator.
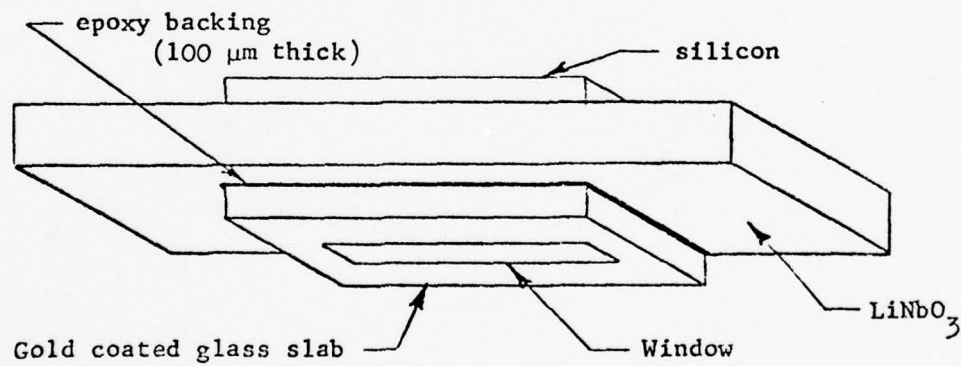
Fig. 2.   Epoxy Backing to Damp Out Spurious Responses.

(a) Coded transducer

450 μm

450 μm

450 μm

100 μm   100 μm
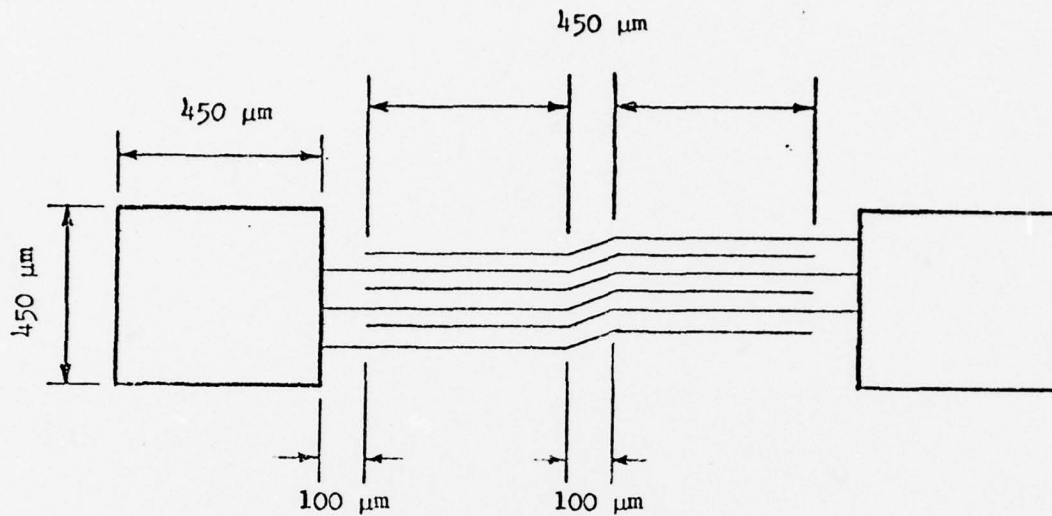
(b) Storage correlator with coded transducers

silicon

2 parallel diode arrays

LiNbO$_3$
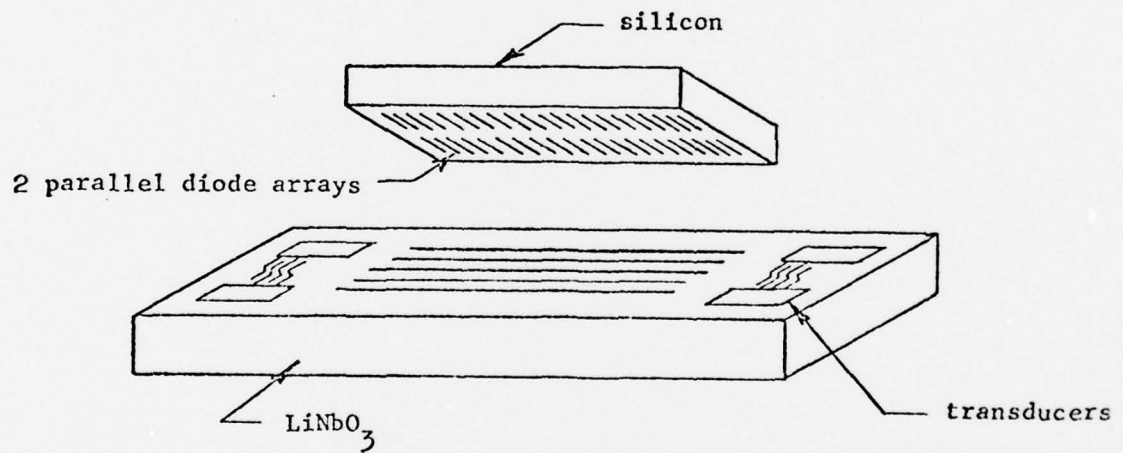
transducers

Fig. 3.   The Coded Transducer Configuration.
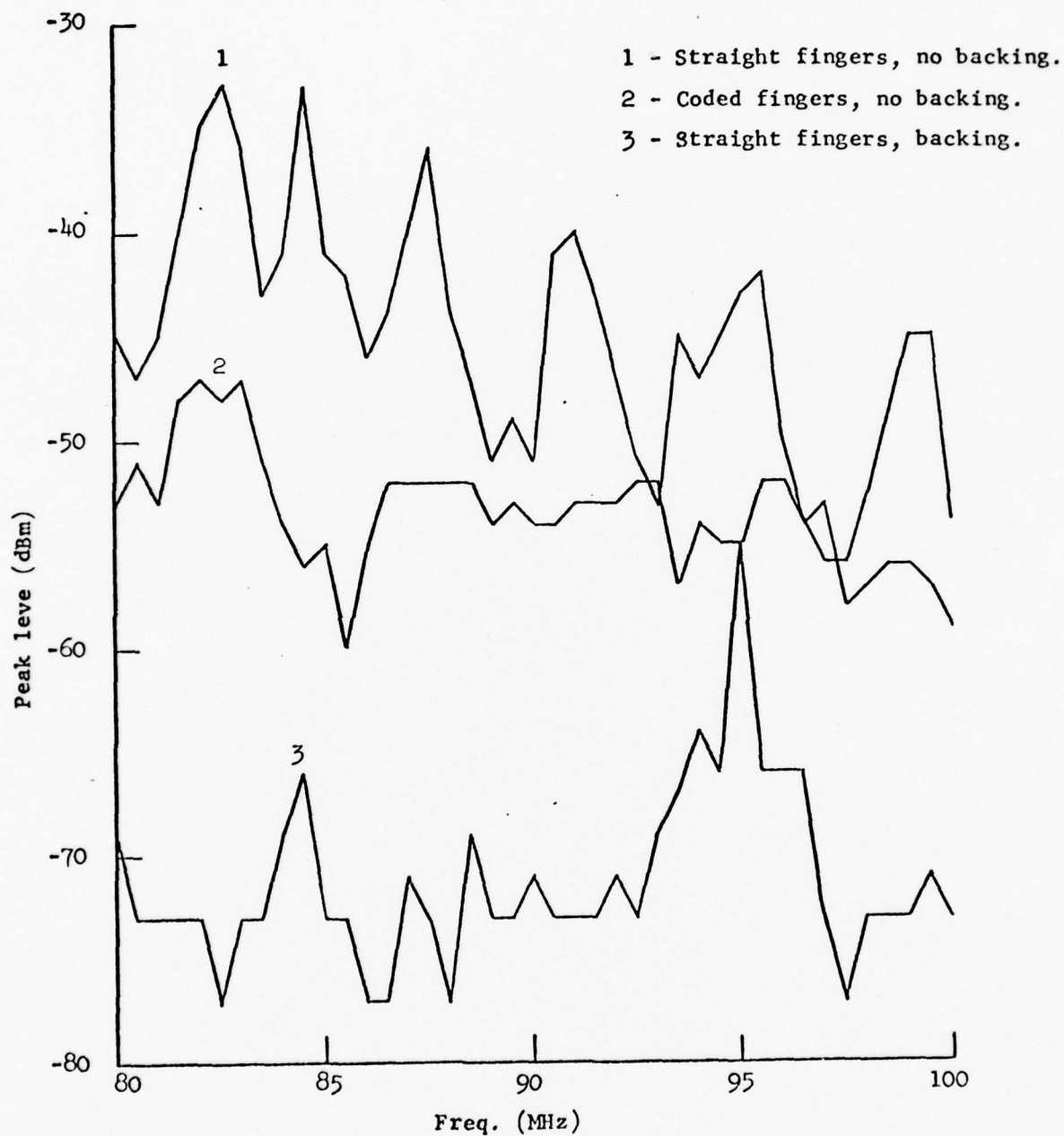
Fig. 4. Relative Spurious Signal Levels
with and without Coded Transducers
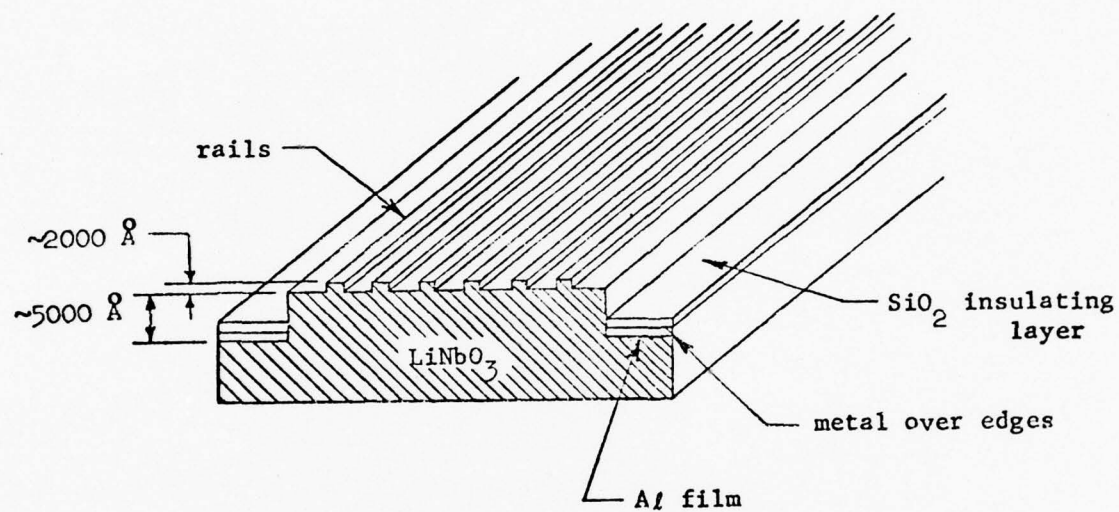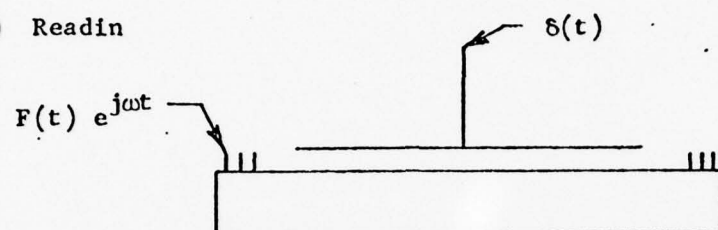and a Damped Backing

rails

~2000 Å

~5000 Å

SiO$_2$ insulating layer

LiNbO$_3$

metal over edges

Aℓ film

Fig. 5.   The Ground Strip Configuration.

(a) Readin

$\delta(t)$

$F(t)\, e^{j\omega t}$

(b) Readout

$G(t)\, e^{j\omega t}$

$\left[\int F(z)\, G(z-z_0)dz\right] e^{j\omega t}$

stored $F(z)\, e^{jkz}$
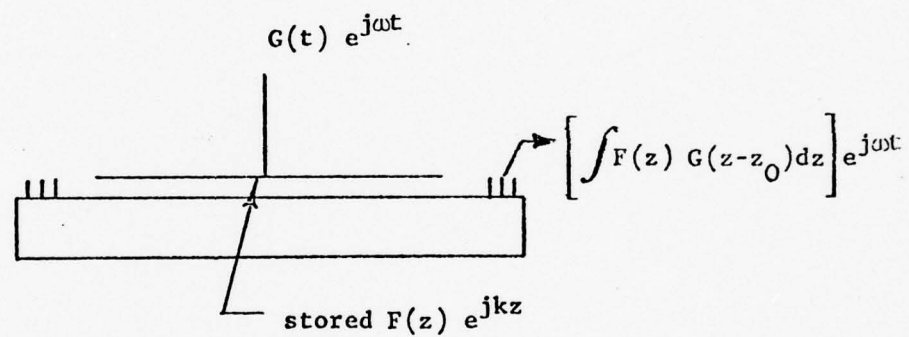
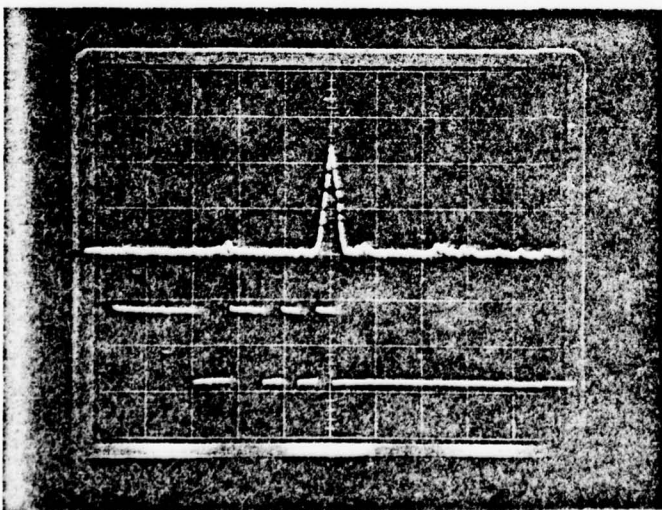Fig. 6. The Pulsed Mode of Operation.
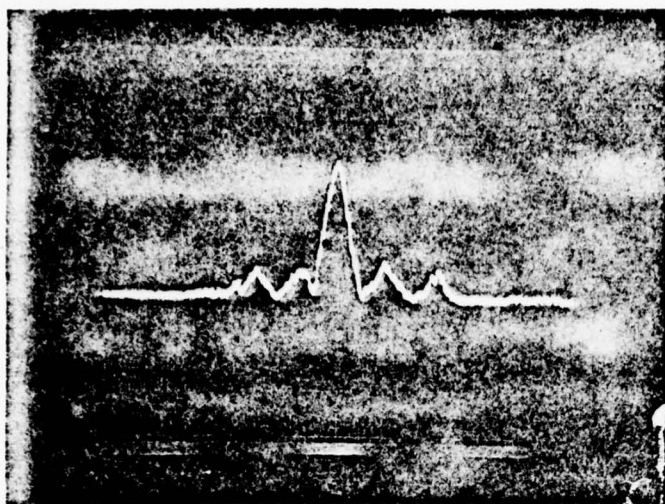
BIPHASE BARKER
CODE CORRELATION

5 BITS: +++−+

(2 μsec/div)

7 BITS: +++−−+−

(2 μsec/div)

13 BITS
+++++−−++−+−+
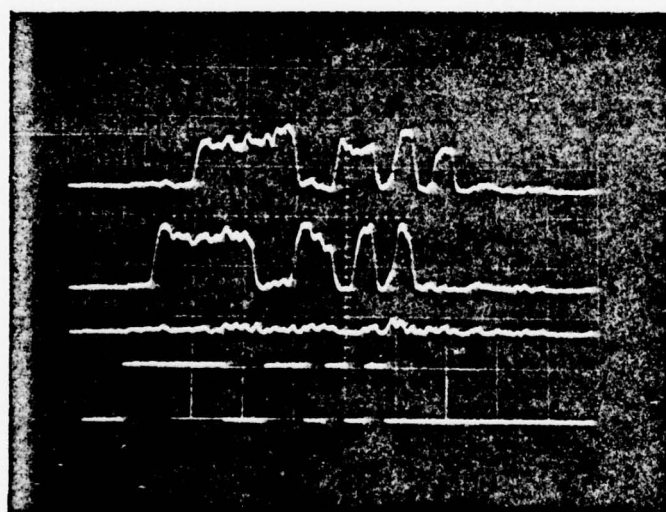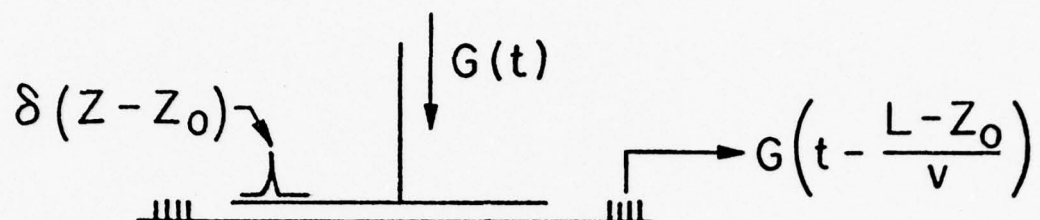
(1 μsec/div)

Fig. 7

- 31 -

3581-3
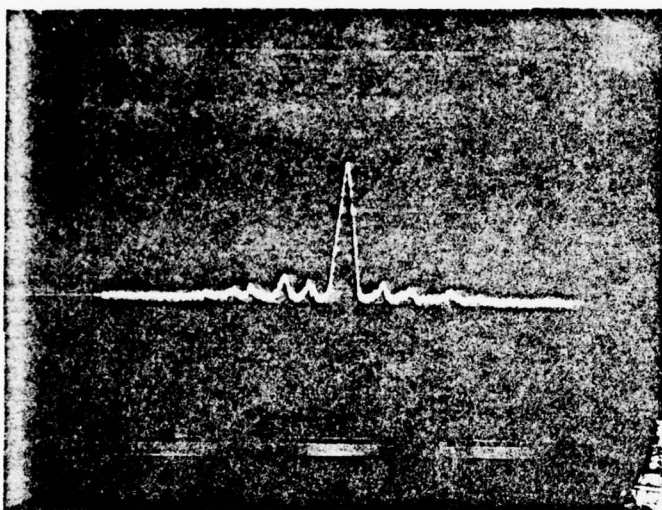
ELECTRONICALLY VARIABLE DELAY
WITH THE STORAGE CORRELATOR

$$\delta(Z-Z_0) \qquad \downarrow G(t) \qquad \rightarrow G\left(t - \frac{L-Z_0}{v}\right)$$

4 μsec DELAY

NO DELAY
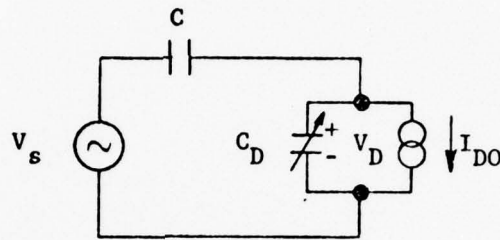NO INPUT

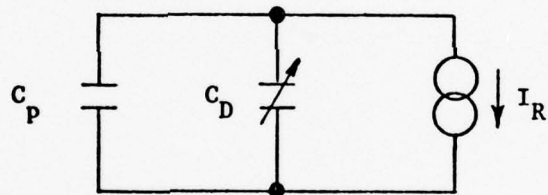INPUT SIGNAL

$\dashv$ $\vdash$ 5μsec

Fig. 8

- 32 -

(a) Complete model
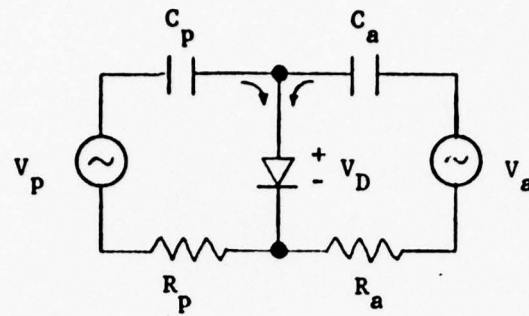
(b) Reduced model

(c) Storage model ($V_s = 0$)
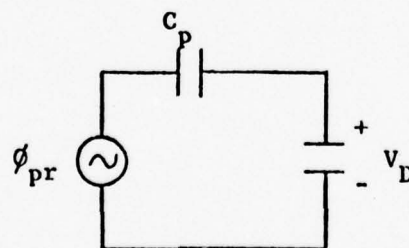

(d) Readout model

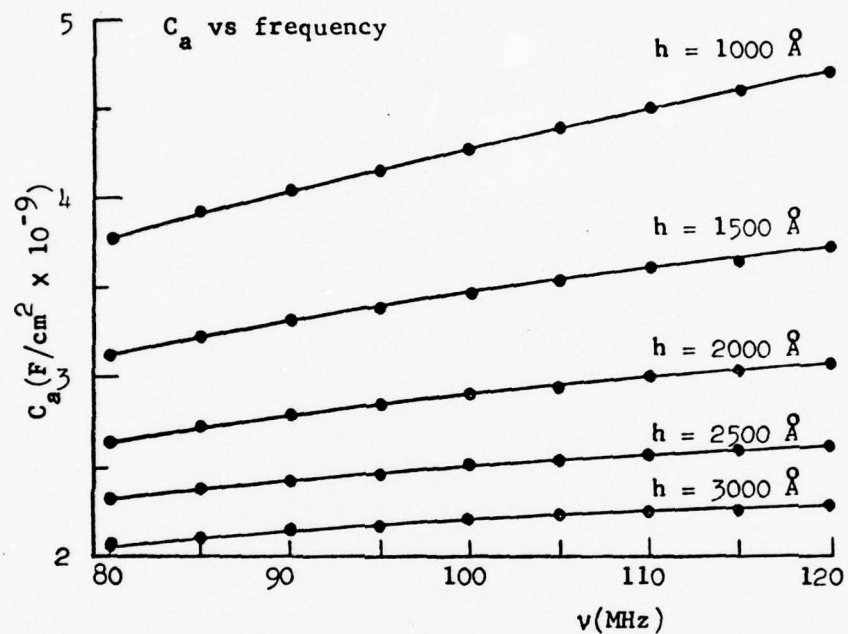Fig. 9. Memory Correlator Equivalent Circuit Models.

- 33 -

Fig. 10. C_a as a Function of Frequency for Various Airgaps.
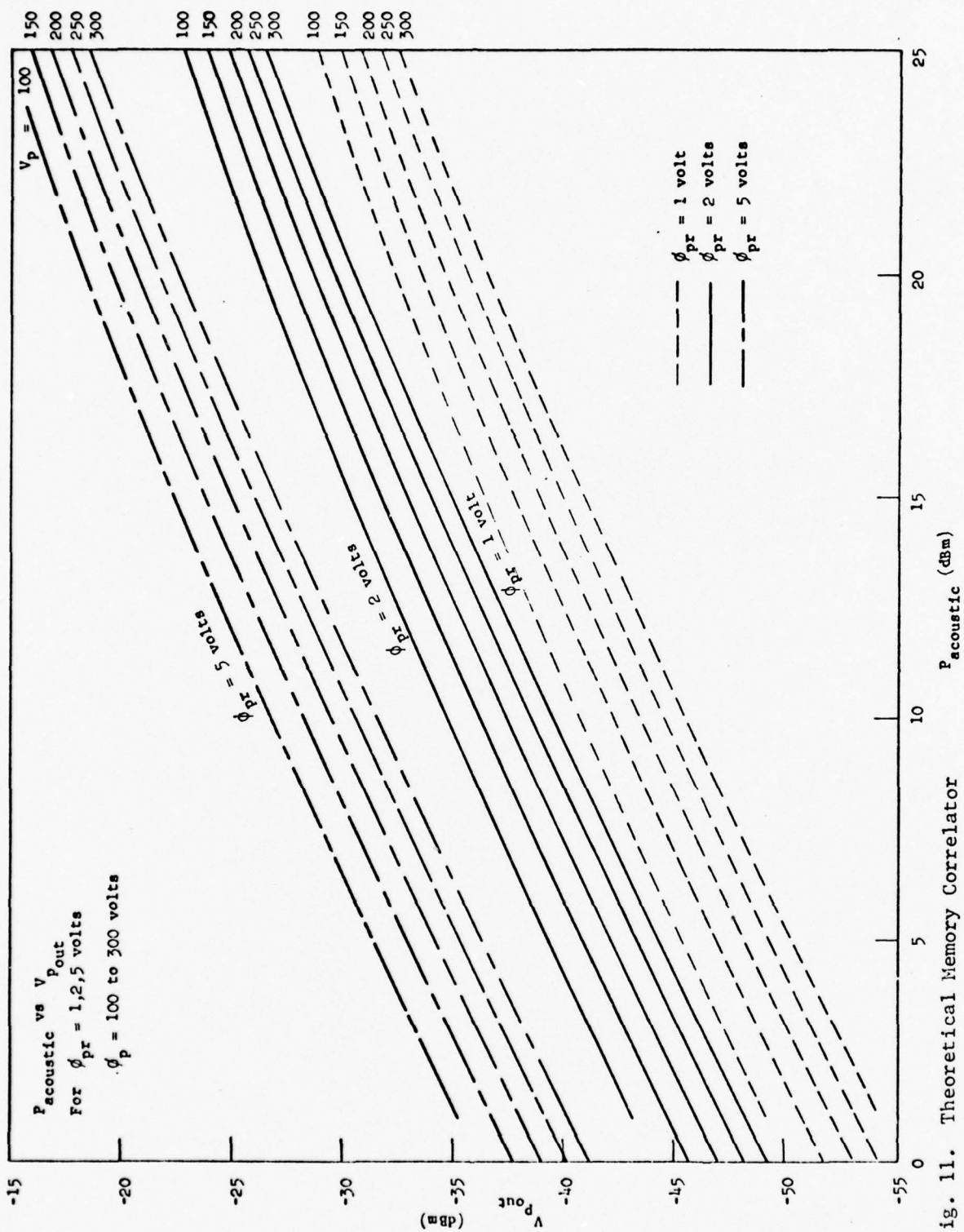
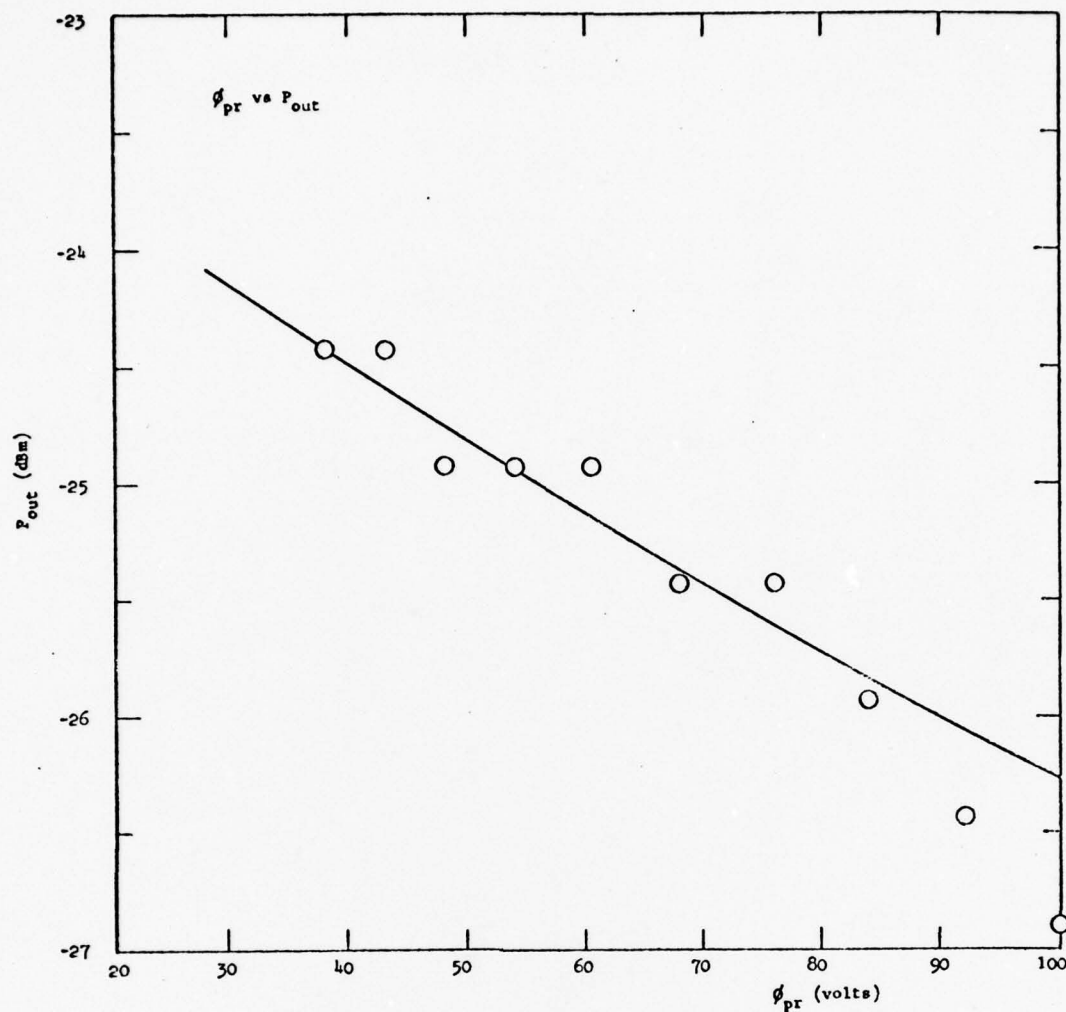Fig. 11. Theoretical Memory Correlator Output Curves.

Fig. 12. Variation of Correlator Output with
Plate Pulse Height, Theoretical and Experimental
P_a = 20 dBm , I.L. = 20 dB (volts).

B. A New Convolver Structure for Optical Imaging

1. Introduction

In our previous progress reports, we have demonstrated that the SAW airgap convolver can be used as an optical imaging device. This device has the unique feature of being capable of obtaining the spatial Fourier transform of an optical image. But it also suffers from the lack of dynamic range, due to the presence of a large "dark current" signal. In order to overcome this problem, more sophisticated signal processing techniques have to be resorted to, such as time gating the spatial Fourier transform of the optical image to remove the low spatial frequency components of the image, or operating the convolver in the nondegenerate mode. Both techniques involve the use of a great deal of equipment and critical adjustments, and, thus, have lost some of their practicality. In this part of the report, a new convolver structure for optical imaging is described. This is easy to operate, and utilizes the charge storage capability of the p-n junction diode array. So it provides good light sensitivity and dynamic range.

In Sections 2 and 3, a brief review of the use of the p-n diode convolver for optical imaging is given. This review should provide enough background for Section 3, where the new structure and its operating principles will be described. Section 4 will describe how this structure is applied to optical imaging. Section 5 will give some preliminary experimental results.

2. The Operation of a Stored Charge p-n diode Convolver and Its Application to Optical Imaging

The use of an integrated diode array in the airgap convolver structure has been discussed rather thoroughly in our last progress report. The

- 37 -

detailed structure and a complete theory of such a convolver can be found in Joly's Ph.D. thesis, which accompanied our last report. For such a convolver, which is shown schematically in Fig. 1, the convolution output V_3 at frequency $\omega_1 + \omega_2$, when the two acoustic signals are at frequencies ω_1 and ω_2, respectively, is found to be

$$V_3 = \frac{1}{2} \frac{\left(\frac{\partial C}{\partial V}\right)_{V_0}}{C_{V_0} + C_p} V_1 V_2 \qquad (2\text{-}1)$$

where C_{V_0} is the depletion capacitance of the p-n junction when it is biased by a voltage V_0, C_p is the effective capacitance of the $LiNbO_3$ slab, V_1 and V_2 are the two surface potentials seen by the diode, due to the two propagating acoustic waves, and $\left(\frac{\partial C}{\partial V}\right)_{V_0}$ is the rate of change of the diode depletion capacitance versus the bias voltage evaluated at the bias level V_0.

It will be seen from Eq. (2-1), that the output voltage of the convolver depends on the bias potential. Typically, this decreases rapidly with the bias potential. So the convolver efficiency can be changed by change of bias. In practice, because there are no direct connections to the convolver diodes, this implies using a pulsed bias. Thus, we can bias the diodes negative, and decrease the efficiency by application of a sufficiently large pulse bias. On the other hand, by biasing the diode into forward current with a positive bias, when the bias voltage decreases to zero, the diode will assume a negative potential for the total storage time. This can give rise to larger negative biases for a given externally applied voltage than in the first case. Furthermore, this negative bias

- 38 -

remains for a storage time which is determined by the illumination present on the diode. When the diode is illuminated, there will be a leakage current associated with the electron hole pairs generated, and so the convolution efficiency will change with the light level. In practice, this implies that a large dynamic range can be obtained if sufficienctly large negative biases can be generated. In this section, we use the technique already described in Section A with electrodes on the top of the acoustic surface wave delay line to obtain a relatively large pulse biases of the order of 10 - 30 V , and a $\sim$nic range of as much as 30 dB .

3. <u>Theory of the p-n Diode Stored Charge Convolver</u>

For a p^+-n step junctions,

$$
C_{V_0} = \sqrt{\frac{qN_d\epsilon_s}{2(V_b - V_0)}} = \sqrt{\frac{qN_d\epsilon_{si}}{2V_b(1 - V_0/V_b)}} = \frac{C_0}{\sqrt{1 - V_0/V_b}} \tag{2-2}
$$

where V_b is the built-in potential of the $p - n$ junction and

$$
C_0 = \sqrt{\frac{qN_d\epsilon_{si}}{2V_b}}
$$
is the capacitance of the diode at zero bias. From

Eq. (2-2), $A = \left.\dfrac{\partial C}{\partial V}\right|_{V_0}$ can be calculated easily.

$$
A = \frac{1}{2V_b} \frac{C_0}{(1 - V_0/V_b)^{3/2}} \tag{2-3}
$$

In order to obtain the full expression for V_3 , the two potentials V_1 and V_2 seen by the diodes must be related to the acoustic potentials ϕ_{a1} and ϕ_{a2} associated with the two acoustic waves. By using the simplified model as shown in Fig.15, the following relationships can readily be derived.

- 39 -

$$V_1 = \frac{C_g}{C_g + C_{V_0}} \phi_{a1} \quad , \quad V_2 = \frac{C_g}{C_g + C_{V_0}} \phi_{a2} \qquad (2\text{-}4)$$

where C_g is the air-gap capacitance.

Substituting Eqs. (2-3) and (2-4) into (2-1), the full expression for V_3 is obtained.

$$V_3 = \frac{1}{4V_b} \frac{C_0}{(1 - V_0/V_b)^{3/2}} \frac{C_g^2}{(C_g + C_{V_0})^2} \frac{\phi_{a1}\phi_{a2}}{C_p + C_{V_0}}$$

$$= \left\{ \frac{1}{4V_b} \left(\frac{C_g}{C_0}\right)^2 \right\} \left\{ \frac{1}{\left(1 + \frac{C_p}{C_0}\sqrt{1 - V_0/V_b}\right)\left(1 + \frac{C_g}{C_0}\sqrt{1 - V_0/V_b}\right)^2} \right\} \phi_{a1}\phi_{a2}$$

$$(2\text{-}5)$$

Typical values for a convolver with an airgap of 1500 $\overset{\text{o}}{\text{A}}$ are:

$$V_b = 0.83 \text{ v} \quad (\text{for } 10 \ \rho - \text{cm Si}) \ ,$$

$$C_g = 3550 \text{ pF/cm}^2 \ ,$$

$$C_0 = 7000 \text{ pF/cm}^2 \ ,$$

$$C_p = 90 \text{ pF/cm}^2 \ .$$

We can see immediately from this expression that the output signal at the sum frequency developed across the diodes depends on the bias conditions of the diodes; it goes up with increasing forward bias and drops with increasing reverse bias. Also clear from Eq. (2-5) is that a large dynamic range for the output signal can be obtained only if a large reverse bias can be applied to the diodes. Unfortunately, for the conventional convolver configuration

- 40 -

(see Fig. 1), this is difficult. Due to the thickness of $LiNbO_3$ slab ($\approx 500\,\mu$), a high voltage pulse generator has to be employed to strongly reverse bias the diodes and thus giving a large dynamic range. The top plate configuration already described in Section B is a very suitable one for overcoming this difficulty.

4. The New Structure with Ground Strips on the Upper Surface of the
    $LiNbO_3$

The new convolver configuration is shown in Fig. 5. As can be seen, this new configuration differs from the old one in two respects. First, two $A\ell$ strips which separate from each other by a little more than the acoustic beam width are deposited on the $LiNbO_3$ delay line. Secondly, the p - n junction diodes on the Si slab are made longer to overlap partially with the two metal strips so that a finite capacitance exists between the p - n junctions and the metal strips.

The area of the $LiNbO_3$ crystal where the two $A\ell$ strips sit is further etched back to provide enough room for the $SiO_2/A\ell$ strips. The purpose of the sputtered SiO_2 layers on top of the $A\ell$ strip is to avoid any possible shorts between the p^+ region at the ends of the diodes and the metal strips. As a result of the anisotropic chemical etchant (KOH) we used to cut the V-groove mesa diode structure, sharp corners appear at both ends of the mesa diodes. These sharp corners create a vulnerable situation where both physical damages to the silicon or low voltage dielectric breakdown may occur, thus causing the p^+ regions to be shorted to the metal strips.

The two $A\ell$ strips are electrically grounded as shown in Fig. 5. When a pulse bias is applied to the back of the silicon slab, the diodes will be

- 41 -

capacitively forward biased or reverse biased through the ends of the diodes where they overlap with the ground strips. The important result of the addition of the ground strips is that the applied bias does not drop across the LiNbO$_3$. Since the bulk of the silicon is respectably conductive, most of the applied voltage will now drop across the p - n junction depletion regions in the reverse bias situation, or the diodes can be turned on strongly in the forward bias case.

Due to the overlapping of the ends of the diodes and the ground strips, an extra capacitance C_M should be placed in parallel with C_{V_0} in the equivalent circuit of Fig. 13. This is the only modification that has to be made to obtain the expression for the convolution output of the new configuration. By following exactly the same derivations that leads to Eq. (2-5), we can easily find the equivalent expression for the present structure.

$$V_3 = \left\{ \frac{1}{4V_b} \left(\frac{C_g}{C_0} \right)^2 \right\} \left\{ \frac{1}{\left(1 + \frac{C_M}{C_0} \sqrt{1 - V_0/V_b} \right)} \cdot \frac{1}{\left(1 + \frac{C_g + C_M}{C_0} \sqrt{1 - V_0/V_b} \right)^2} \right\} \varphi_{a1} \varphi_{a2}$$

$$(2-6)$$

In Fig. 14, the convolution output V_3 is plotted as a function of the bias across the diodes. The voltage V_0 is the real drop across the diodes, not the amplitude of the voltage externally measured. The 0 dB reference point in the plot is chosen as the convolution output of a convolver at zero bias of the regular structure without the ground strips. Different curves in this plot represent different amount of overlapping between the diodes and the ground strips.

Depending on the detailed design of the structure, the overlapping capacitance C_M can be an order of magnitude or more larger than the piezoelectric substrate capacitance C_p in Eq. (2-5). Figure 14(a) is for $C_M = 5000$ pF/cm^2 and 14(b) is for $C_M = 10000$ pF/cm^2 .

Two things immediately come to our attention: (1) the convolution output at zero bias will drop slightly for the new structure; the larger the overlapping capacitance, the more the drop, (2) the more the overlapping, the more sensitive the device is to the bias. While keeping the overlap area fixed, the same sensitivity to bias can also be achieved by decreasing the thickness of the sputtered SiO_2 , thus giving C_M a larger capacitance per unit area.

5. Optical Imaging Using the Ground Strip Structure

As mentioned in the last section, when a bias voltage is applied between the back of the Si and the ground, the diodes can be either forward or reverse biased mainly through the overlapping capacitance C_M . The equivalent circuit for the biasing looks simply as shown in Fig. 15 where $C_M \gg C_p$ has been assumed and any series resistance present has been neglected. Also shown in this figure are two techniques used in biasing the diodes for optical imaging applications. One technique uses a short pulse that forward biases the diodes during its presence. The other technique involves the use of a long pulse that reverse biases the diodes during its presence. Since the physics behind the two techniques is almost exactly the same, only the first technique will be discussed in detail below, and the extension of the result to the second technique should be straight-forward.

Let a short negative pulse of amplitude V_p be applied to point B in

Fig. 15. Initially the diode is strongly forward biased and a large current flows to charge up the capacitor C_M. The current will drop very quickly as more of the applied voltage is dropped across the capacitor and less is dropped across the diode. Eventually, in a matter of a few microseconds, all the applied voltage V_p appears across the capacitor and the current stops flowing in this state. There is an amount of charge $Q = C_M V_p$ sitting on the capacitor C_M. The bias pulse can now be turned off and point B returns to ground potential. Due to the charge stored in the capacitor C_M, the diode is switched to the reverse bias condition, and the situation becomes like that shown in Fig. 16.

Let Q_1 be the amount of charge that now resides in the depletion layer of the diode and $Q - Q_1$ be the amount of charge left on the capacitor C_M. If each diode has an area of A_d, then the depletion layer charge per unit area is Q_1/A_d. Equating the potential drop across the capacitor and across the diode, we get

$$\frac{Q - Q_1}{C_M} = V_d(Q_1/A_d) .$$

(2-7)

where $V_d(Q_1/A_d)$ is the potential drop across a p^+ n junction when the depletion layer charge density is Q_1/A_d.

It is known in p - n junction theory that the voltage drop across a diode V_j is given by

$$V_j = \frac{qN_d x_n^2}{2\epsilon_{si}}$$

(2-8)

where N_d is the doping density of the n-type substrate and x_n is the depletion layer width.

In thermal equilibrium, there is a built-in potential V_b across the diode and there is an amount of charge Q_0 in the depletion layer of width x_0 . Equation (2-8) then becomes

$$V_b = \frac{qN_d x_0^2}{2\epsilon_{si}} = \frac{(qN_d x_0)^2}{2qN_d\epsilon_{si}} = \frac{Q_0^2}{2qN_d\epsilon_{si}} \tag{2-9}$$

where the relation $Q_0 = qN_d x_0$ has been used.

Equation (2-9) can again be used when an extra amount of charge Q_1/A_d is added to the depletion region.

$$V_b + V_d(Q_1/A_d) = \frac{(Q_0 + Q_1/A_d)^2}{2qN_d\epsilon_{si}} \tag{2-10}$$

Subtracting Eq. (2-9) from (2-10), we have

$$V_d(Q_1/A_d) = \frac{\left(\frac{Q_1}{A_d}\right)\left(\frac{Q_1}{A_d} + 2Q_0\right)}{2qN_d\epsilon_{si}} = \frac{\left(\frac{Q_1}{A_d}\right)\left(\frac{Q_1}{A_d} + 2\sqrt{2qN_d\epsilon_{si}V_b}\right)}{2qN_d\epsilon_{si}} \tag{2-11}$$

Substituting Eq. (2-11) into Eq. (2-7),

$$\frac{Q - Q_1}{C_M} = \frac{\left(\frac{Q_1}{A_d}\right)\left(\frac{Q_1}{A_d} + 2\sqrt{2qN_d V_b \epsilon_{si}}\right)}{2qN_d\epsilon_{si}} \tag{2-12}$$

Since $Q = C_M V_p$. Eq. (2-12) becomes

$$V_p - \frac{Q_1}{C_M} = \frac{\left(\frac{Q_1}{A_d}\right)\left(\frac{Q_1}{A_d} + 2\sqrt{2qN_d V_b \epsilon_{si}}\right)}{2qN_d\epsilon_{si}} \tag{2-13}$$

Let $Q_1/A_d \overset{d}{=} Q_1'$, $2qN_dV_b\epsilon_{si} \overset{d}{=} p^2$, $V_p/V_b \overset{d}{=} \alpha$, and $A_d/C_MV_b \overset{d}{=} \beta$, then Eq. (2-13) becomes

$$Q_1' + (2p + p^2\beta)Q_1' - p^2\alpha = 0 \quad . \tag{2-14}$$

This is a quadratic equation in Q_1' , and the solution that makes Q_1' a positive quantity is

$$Q_1' = \frac{-(2p + p^2\beta) + \sqrt{(2p + p^2\beta)^2 + 4p^2\alpha}}{2} \tag{2-15}$$

Therefore, right after the biasing pulse is turned off, the p - n junction is not reverse biased to the full amplitude of the original pulse, but instead it is reverse biased by an amount determined by substituting Eq. (2-15) into (2-11).

$$V_d = \frac{Q_1'(Q_1' + 2p)V_b}{p^2} \tag{2-16}$$

Fig. 17 is a plot of the reverse bias voltage V_d across the diodes versus the amplitude of the original forward bias. It has been assumed in this plot that 20% of the diode area overlaps with the ground metals. Different curves in the plot represent different values per unit area of C_M which can be varied by controlling the depth to which the $LiNbO_3$ has been sputter etched and the thickness of the sputtered SiO_2 on the Aℓ strips. For a structure where the $LiNbO_3$ has been etched 5000 Å deep and the sputtered SiO_2 film and the Aℓ underlayer are 2500 Å and 1500 Å thick, respectively, the overlapping capacitance per unit area is about

- 46 -

2800 pF/cm^2 . So the difference in amplitude between the actual reverse
bias that can achieved using this bias technique and the original forward
bias is quite appreciable, as can clearly be seen from the plot. But, as
compared to the configuration without the ground strips, this structure
gives at least an order of magnitude improvement.

The situation immediately after the bias pulse is turned off can, there-
fore, be depicted as a capacitor being discharged through a reverse biased
diode, as shown in Fig. 18. The discharging current $I_D(V_d)$ is the leakage
current of the diode under a reverse bias V_d . Since the leakage current
of a well-fabricated diode in the dark is small, the diode should stay re-
verse biased for a long time. As a function of time, the reverse bias vol-
tage across the diode should satisfy the following equation:

$$V_d(t) = V_d(t = 0) - \frac{1}{C_M} \int_0^t I_D dt = V_d(t = 0) - \frac{I_D t}{C_M} \qquad (2\text{-}17)$$

where we have assumed that the leakage current is independent of the reverse
bias.

From our previous discussion, i.e., Eq. (2-6), we know that the convo-
lution output depends on the bias condition of the diodes, so we can expect
the convolution output to be weak at the beginning and gradually rises to its
full strength as the diodes recover from being reverse biased to their thermal
equilibrium condition according to Eq. (2-17).

Therefore, it is established that the decay time of the stored charge
on the capacitor C_M , or the recovery time of the convolution, is directly
fixed by the reverse current of the diode. If light is now shone on the diode
array through the transparent LiNbO$_3$ crystal, the electron-hole pairs gene-

rated by the illumination will affect drastically the reverse current and thus accelerate the recovery rate of the convolution output. So, at a time T after the turning off of the charging pulse, the charge remaining on the capacitor C_M, or the amplitude of the convolution output will be characteristic of the illumination level. Because the diodes in our mesa-structured diode array are well isolated from each other, the profile of the remaining charge is the replica of the illumination pattern.

When the diodes are illuminated, Eq. (2-17) should be modified to become

$$V_d(x,T) = V_d(t=0) - \frac{1}{C_M} \int_0^T I_{ph}(x,t)dt \qquad (2-18)$$

where the magnitude of the photo current I_{ph} depends on the spectrum of the illumination, the depletion layer width, and the local light intensity. It should be noted that the bias on each diode is a function of both the intensity of the local illumination and the time elapsed. Therefore, this device does not sense the illumination by giving its instantaneous response to light, but instead it senses the effect of light by integrating the effect over a time T.

The scanning of the illumination profile can then be achieved by feeding a long RF pulse to one end of the LiNbO$_3$ delay line and a short RF pulse to the other end, as in the so called "Simple Imager" system. Alternatively, we can use a coded function, such as a linear FM chirp, as the scanning signals; then we can obtain image transformation and an improvement of signal to noise ratio can be achieved, by feeding this code into a matched filter.

As a conclusion to this section, it should be emphasized here that due to the integration effect mentioned above the light sensitivity of the device can easily be altered by varying the integration time. For instance, a low light level image can be scanned after a long integration period T. Hence, this device should give very good light sensitivity.

6. Experimental Results and Conclusions

a. By applying approximately a 35 volt bias voltage, the present system gives a dynamic range of 30 dB . When more bias is applied to the p-n junctions, the depletion layer of each diode extends beyond the bottom of the V-groove and starts to merge with each other, thus giving some undesirable phenomena. By proper processing of the diode array and by increasing the overlapping capacitance C_M to some extent, we would expect at least a further 20 dB increase of dynamic range at a particular sensitivity level.

b. Fig. 19(a) shows the recovery of the convolution output in the dark, after a 15 μsec 32 volt pulse is used to forward bias the diodes. The recovery time constant is about 200 ms . Fig. 19(b) shows the result of the same experiment under $6\mu w/cm^2$ of illumination. The time constant under this circumstance drops to about 15 ms .

In Fig. 20, we plot the recovery time of the convolution output as a function of the light intensity, where the recovery time has been arbitrarily defined as the time needed for the amplitude of the output to reach 63% of the unbiased value. Independent of the light intensity, all the diodes have to reach the same bias condition in order to give the same output. This means the same amount of charge has to leak through the diodes away from the capacitor, as discussed in the last section. Since the magnitude of the leakage current of a reverse biased diode under illumination is proportional to the intensity of the illumination, we would expect the following to be true:

(Light intensity) $\times$ (recovery time of the convolver) = constant = K .
This represents a straight line, with slope 1 on a log-log scale. Such a line is drawn in Fig. 20 , where the parameter K is taken to be equal to

0.11 μjoule/cm^2 . The deviations of the experimental result from

this straight line at both high and low levels of illumination are be-

lieved to be due to the change of the spectrum of the light source used,

as the illumination intensity is varied.

c. Fig. 21 shows the convolution output as a function of time under

different levels of illumination. Though we cannot see from this plot,

all three curves should start from the origin of the plot. This implies

that the initial recovery rate of the diodes is fast, and it slows down

as time progresses.

d. Fig. 22 plots the convolver output as a function of illumination

levels for fixed integration times. The two integration times chosen for

this plot are 1 ms and 10 ms . This provides us with information on
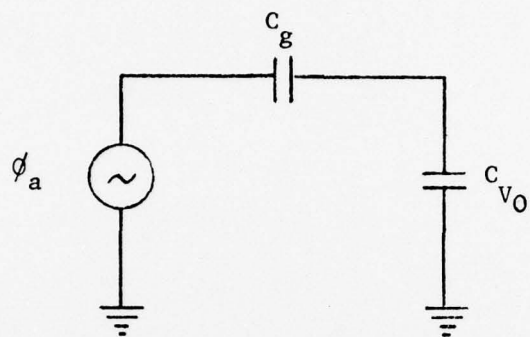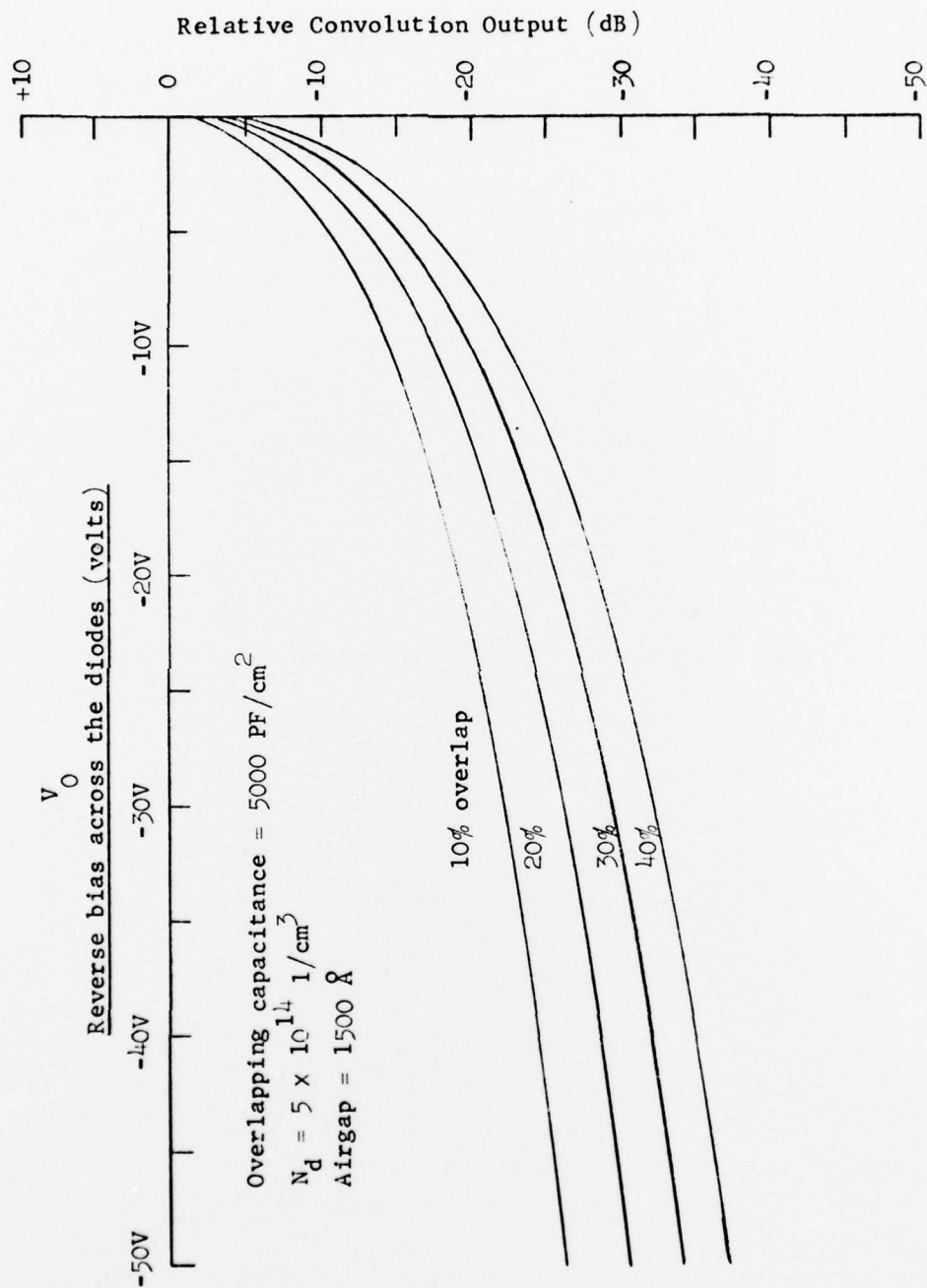
the optimum time for scanning.

Fig. 13

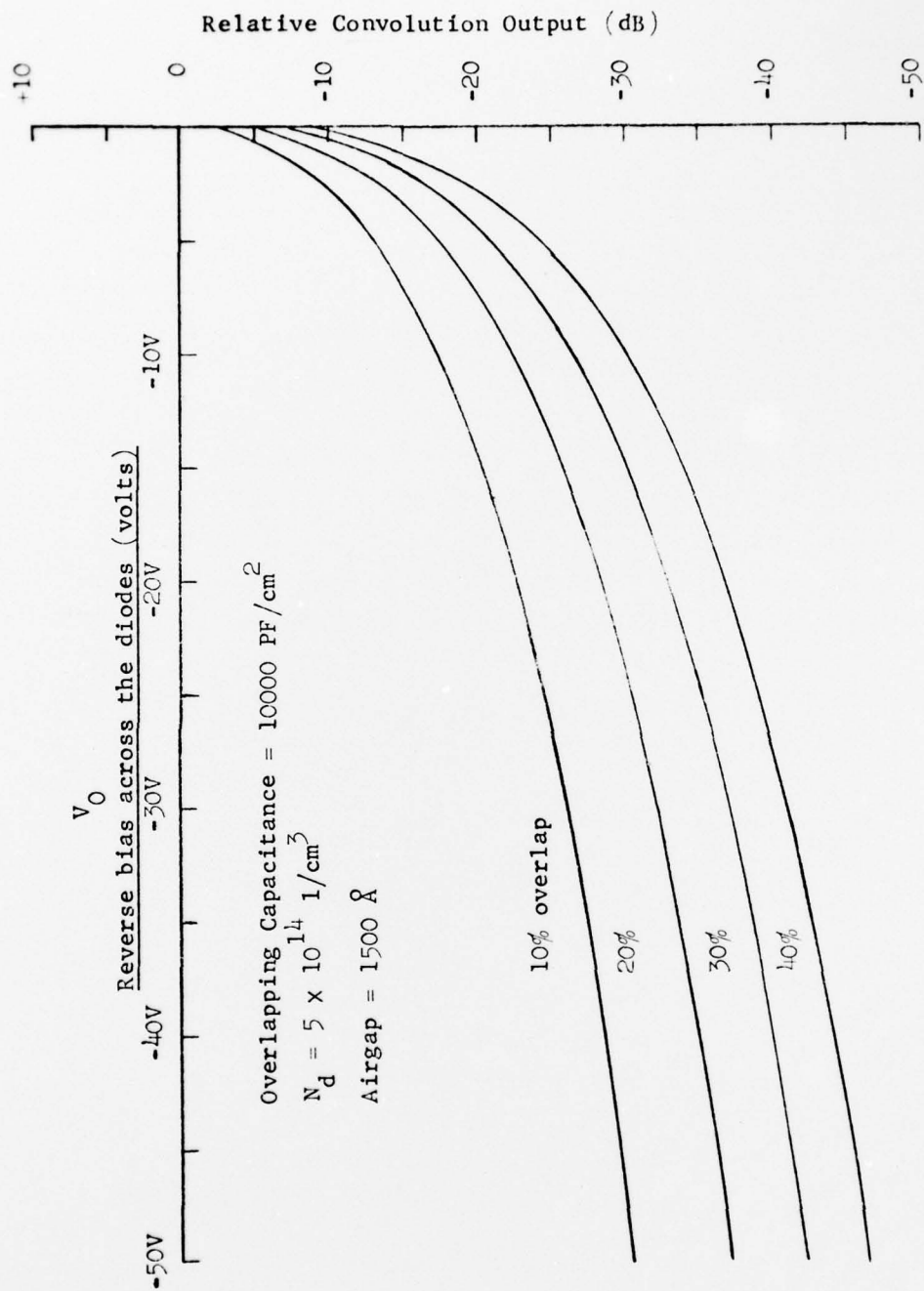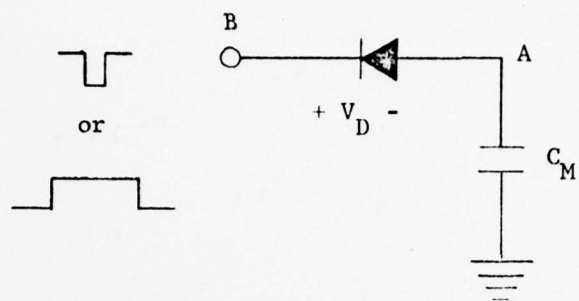Relative Convolution Output (dB)

V_O

Reverse bias across the diodes (volts)

Overlapping capacitance = 5000 PF/cm^2

$N_d = 5 \times 10^{14}$ 1/cm^3

Airgap = 1500 Å

10% overlap

20%

30%

40%

Fig. 14(a)

Relative Convolution Output (dB)

V_o
Reverse bias across the diodes (volts)

Overlapping Capacitance = 10000 PF/cm^2

$N_d = 5 \times 10^{14}$ 1/cm^3

Airgap = 1500 Å

10% overlap

20%

30%

40%

Fig. 14(b)

Fig. 15

Fig. 16

20% Overlap

$N_d = 5 \times 10^{14} \ 1/cm^3$

12500 PF/cm^2

10000 PF/cm^2

7500 PF/cm^2

5000 PF/cm^2

$C_M = 2500 \ PF/cm^2$

Amplitude of the reverse bias across the diodes (volts)

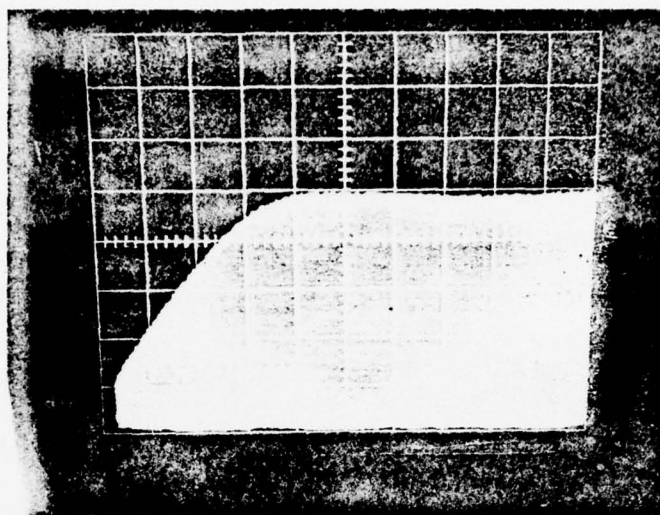Amplitude of the original short bias (volts)

Fig. 17

Fig. 18

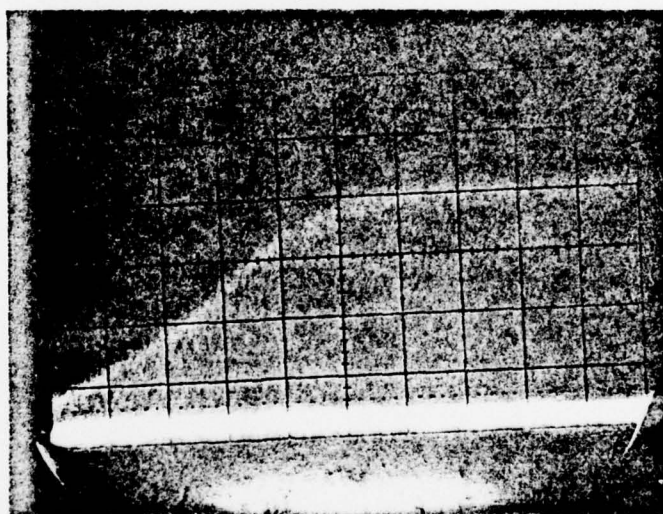Fig. 19(a) Recovery of convolution in the dark (0.1 sec/div)

Fig. 19(b) With $6 \ \mu w/cm^2$ of illumination (5ms/div)

- 57 -

Fig. 20

Light intensity (μw/cm^2)

Recovery Time of the Convolver

Time (ms)

Fig. 21

Relative Convolution Output (dB)

$10\mu w/cm^2$

$5\mu w/cm^2$

$1\mu w/cm^2$

Fig. 22

Relative Convolution Output (dB)
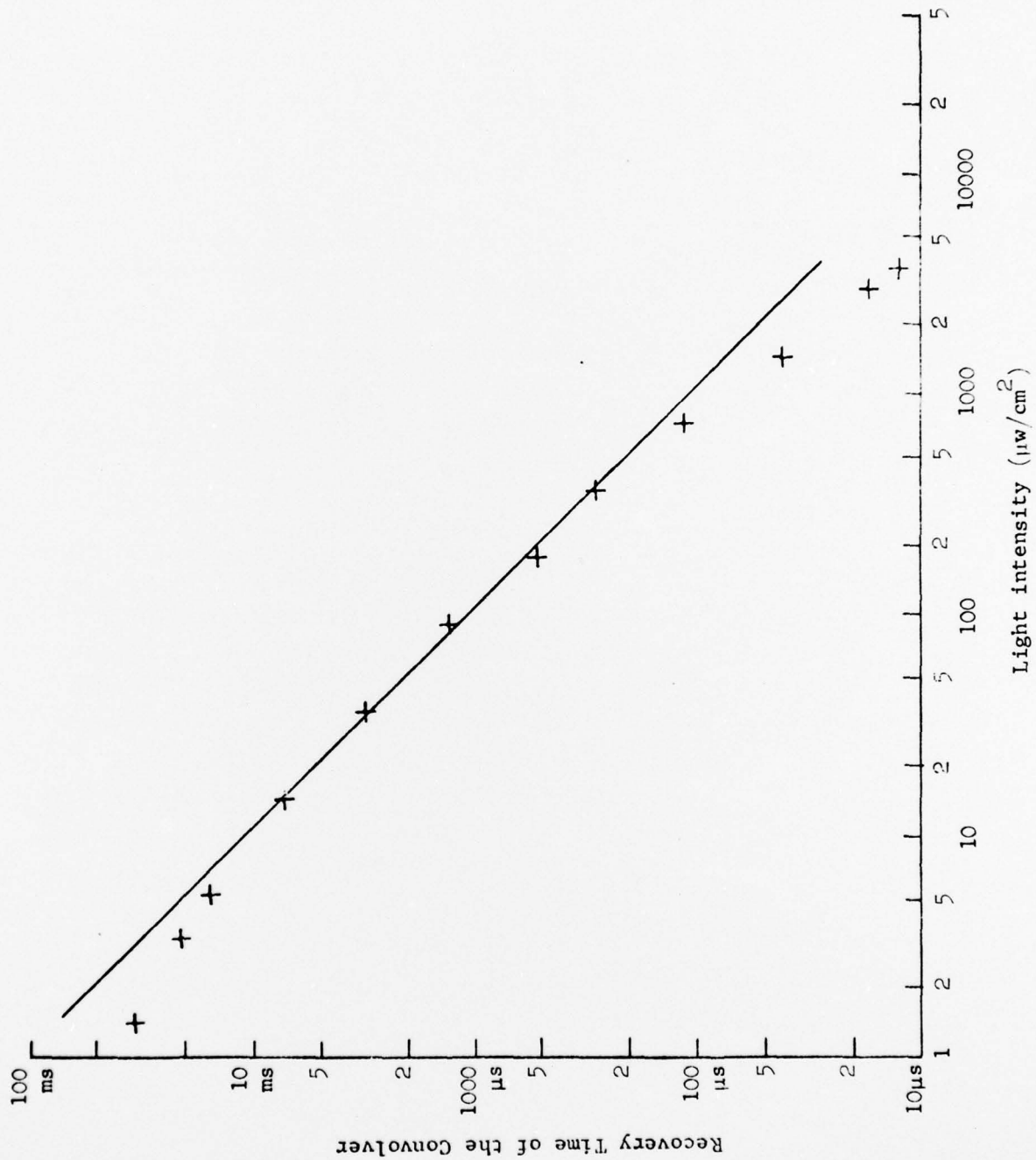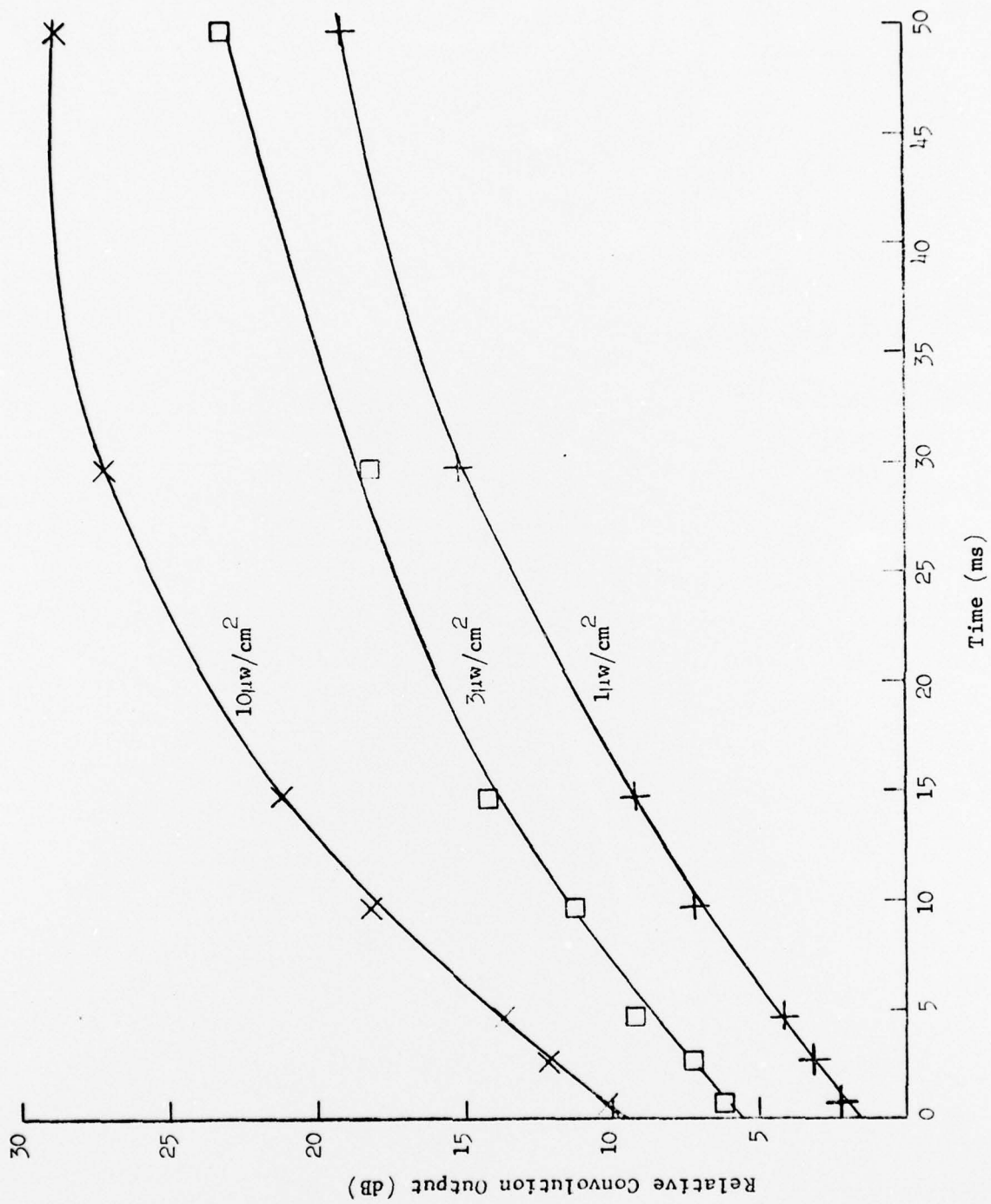
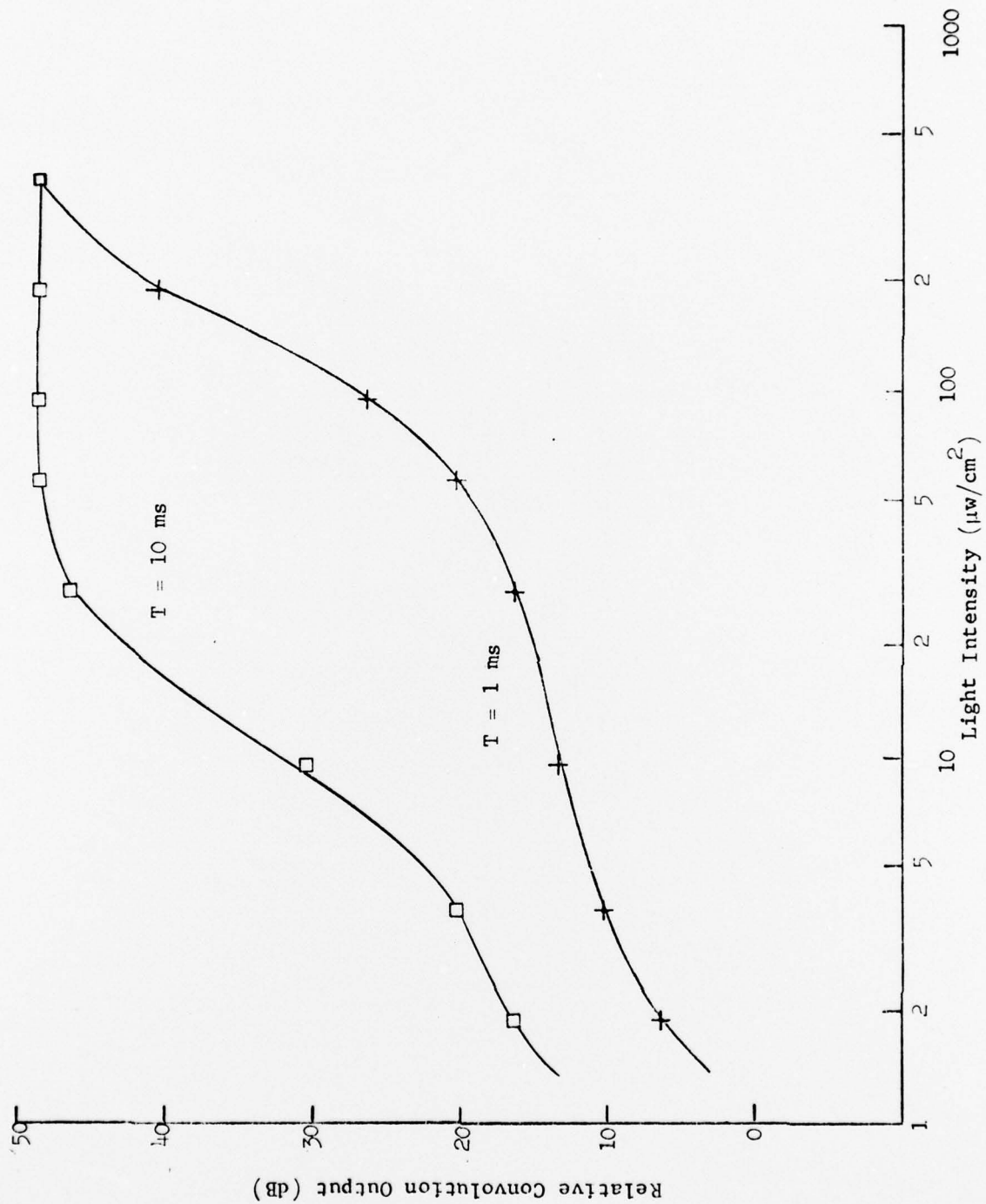Light Intensity ($\mu w/cm^2$)

T = 10 ms

T = 1 ms

- 61 -

C. ZnO on Si Device

We have been pursuing our work on a ZnO on Si storage correlator somewhat less intensively than the airgap convolver studies.

Our main problem in this reporting period has been with the ZnO technology. We have made several changes in our sputtering stations; these were aimed at simplifying its operation, reducing the actual running time, and increasing the yield. We can presently clean our substrates, deposit the gold layer at the edges of the device, and deposit the zinc oxide on the same day. The quality of zinc oxide films on gold has been excellent and reproducible in every run. The quality of the zinc oxide films on silicon dioxide has been good, but not excellent. We are still trying to improve it. We have, however, manufactured zinc oxide on silicon devices with planar p^+ n junction diode arrays. The typical insertion loss of one of these devices was 18 dB with a convolution efficiency of -80 dBm . The reason for the low efficiency was observed in the nonuniformity of the interaction region. A difference in efficiency of about 15 dB existed between one end of the interaction region and the other. The same behavior was observed on the four devices made in that run. We have made a reflection electron diffraction study on one of these devices to determine the quality of the ZnO on both sides of the interaction region; as expected, the quality on one side was poorer than the other. All the indications are that a nonuniform thermal contact was made to the devices while ZnO deposition was taking place. A poor contact would yield to a variation in the substrate temperature across the device and a decrease in the quality of the ZnO film. We will make some more devices with improved

thermal contact during the ZnO deposition.

At the time of writing, we have made the first storage correlation experiments with these devices. We have observed a storage time of the order of 10 m/sec . This is the first time that storage has been observed with a zinc oxide on silicon device with a planar $p^{+}n$ junction diode array.

We are very encouraged by our latest results and we are presently making new devices, where we hope to achieve more efficiency and longer storage times.